

Article

# Landslide Susceptibility Modeling Using Integrated Ensemble Weights of Evidence with Logistic Regression and Random Forest Models

Wei Chen <sup>1,2,3,\*</sup>, Zenghui Sun <sup>1,2,†</sup> and Jichang Han <sup>1,2,\*</sup>

<sup>1</sup> Key Laboratory of Degraded and Unused Land Consolidation Engineering, Ministry of Land and Resources of China, Xi'an 710075, China

<sup>2</sup> Shaanxi Provincial Land Engineering Construction Group Co. Ltd., Xi'an 710075, China; sunzenghui061@126.com

<sup>3</sup> College of Geology & Environment, Xi'an University of Science and Technology, Xi'an 710054, Shaanxi, China

\* Correspondence: chenwei0930@xust.edu.cn (W.C.); hanjc\_sxdj@126.com (J.H.)

† These authors contribute equally to this paper.

Received: 19 November 2018; Accepted: 27 December 2018; Published: 4 January 2019



**Abstract:** The main aim of this study was to compare the performances of the hybrid approaches of traditional bivariate weights of evidence (WoE) with multivariate logistic regression (WoE-LR) and machine learning-based random forest (WoE-RF) for landslide susceptibility mapping. The performance of the three landslide models was validated with receiver operating characteristic (ROC) curves and area under the curve (AUC). The results showed that the areas under the curve obtained using the WoE, WoE-LR, and WoE-RF methods were 0.720, 0.773, and 0.802 for the training dataset, and were 0.695, 0.763, and 0.782 for the validation dataset, respectively. The results demonstrate the superiority of hybrid models and that the resultant maps would be useful for land use planning in landslide-prone areas.

**Keywords:** landslide; weights of evidence; logistic regression; random forest; hybrid model

## 1. Introduction

Landslides are common geological hazards caused by multiple factors including landform [1,2], geological evolution [3], groundwater [4], land use type [5], precipitation [6,7], irrigation [8], earthquake [9], engineering construction [10], and climate change [11–13]. To avoid casualties caused by landslides and guarantee the stable development of mountainous areas, it is critical to determine a control and prevention scheme for landslides in a region. Generally, regional landslide susceptibility maps are beneficial to mitigate the effects of landslide hazards.

At present, various methods have been proposed and introduced into landslide susceptibility mapping. The existing modeling approaches can be put into two categories: qualitative approaches and quantitative approaches [14,15]. In recent years, conventional qualitative approaches have been gradually abandoned by many researchers due to the risk that expert opinion can make the results stray from objective reality [16]. Compared with qualitative approaches, quantitative approaches are mainly based on the hidden information of objective data instead of subjective experience. Additionally, quantitative approaches mainly include traditional mathematical statistic methods, deterministic models, and some state-of-the-art machine learning algorithms.

For traditional statistical methods, the probability-frequency ratio (FR) [17,18], weight of evidence (WoE) [19,20], statistical index (SI) [21,22], index of entropy (IoE) [23,24], certainty factors (CF) [25–27], evidential belief function (EBF) [28–30], and logistic regression (LR) [31,32] models have been

extensively adopted in landslide susceptibility mapping. However, one limitation for all traditional statistical methods is that some hypotheses exist [33]. In deterministic models, the detail characteristics of slopes are necessary to construct the calculation model [34]. Although deterministic models conform to basic physical laws of landslide, these models are not very suitable for regional landslide susceptibility assessments due to the complex process of modeling and computing [34].

In the past decade, with the rise of machine learning and data mining, a number of relevant algorithms have been developed for landslide susceptibility zonation [35–39]. For instance, the logistic regression model (LRM), artificial neural network (ANN), support vector machine (SVM), and decision tree (DT) were the top four machine learning algorithms in landslide susceptibility mapping during the period of 2005–2016 [16]. It is clear that machine learning algorithms improve the prediction accuracy of regional landslide occurrence, but the generalization performance of single classifiers still needs to be promoted [40]. In this way, a series of ensemble approaches have recently become more and more popular in geo-hazard susceptibility mapping [37,41–43].

In terms of ensemble approaches, several single classifiers have been combined using ensemble frameworks including random subspace [44], random forest [45,46], Bagging [47], AdaBoost [48], MultiBoost [49], and so on [37,50–52]. Currently, some novel ensemble techniques have been proposed and applied in landslide susceptibility assessment, flood susceptibility mapping, and groundwater potential analysis [41,53,54]. Additionally, the excellent performance of ensemble algorithms on predictive ability and generalization capacity has also been proven. For example, Kadavi et al. [55] compared four ensemble-based machine learning models (AdaBoost, LogitBoost, Multiclass Classifier, and Bagging) with the traditional frequency ratio model (FRM) in the task of landslide susceptibility mapping. Furthermore, the results demonstrated that all of the AUC values of the four ensemble-based machine learning models were higher than that of FRM. In addition, many scholars preferred to construct ensemble learning models by integrating machine learning algorithms with bivariate statistical models because some of the hypotheses of the conventional models can be weakened through hybrid models [56]. Meanwhile, part of the merits of bivariate statistical models and machine learning models can remain by integrating together. Weights of evidence models, as a classic bivariate statistical approach, can calculate the weights of various categories of a conditioning factor based on sturdy mathematical theories [57]. Furthermore, the weights of evidence models can be integrated with other machine learning approaches to reveal the hidden correlations between different conditioning factors and landslide occurrence. Therefore, in the present study, based on GIS tools, the integrated ensemble weights of evidence with logistic regression and random forest models were employed to map landslide susceptibility, and the results were compared and analyzed quantitatively by receiver operating characteristic curves (ROC) and area under the curve (AUC).

## 2. Study Area

The study area was located in Shaanxi Province, China (Figure 1) where the average annual temperature is 14.2 °C, the average annual rainfall is 909.8 mm, and the evaporation is 1537.1 mm. Topographically, the study area is part of the Qinba Mountain. The general trend is high in the south and low in the north. Elevation ranges from 442 m to 2410 m above sea level, with an average elevation of 1171 m. Slope angles in the study area are in the range of 0 to 70°. Most of the slope angles are in classes of 10–20° (29.27%), followed by 20–30° (26.29%), 0–10° (23.64%), and 30–40° (14.99%). Only 5.81% of slope angles are higher than 40°.

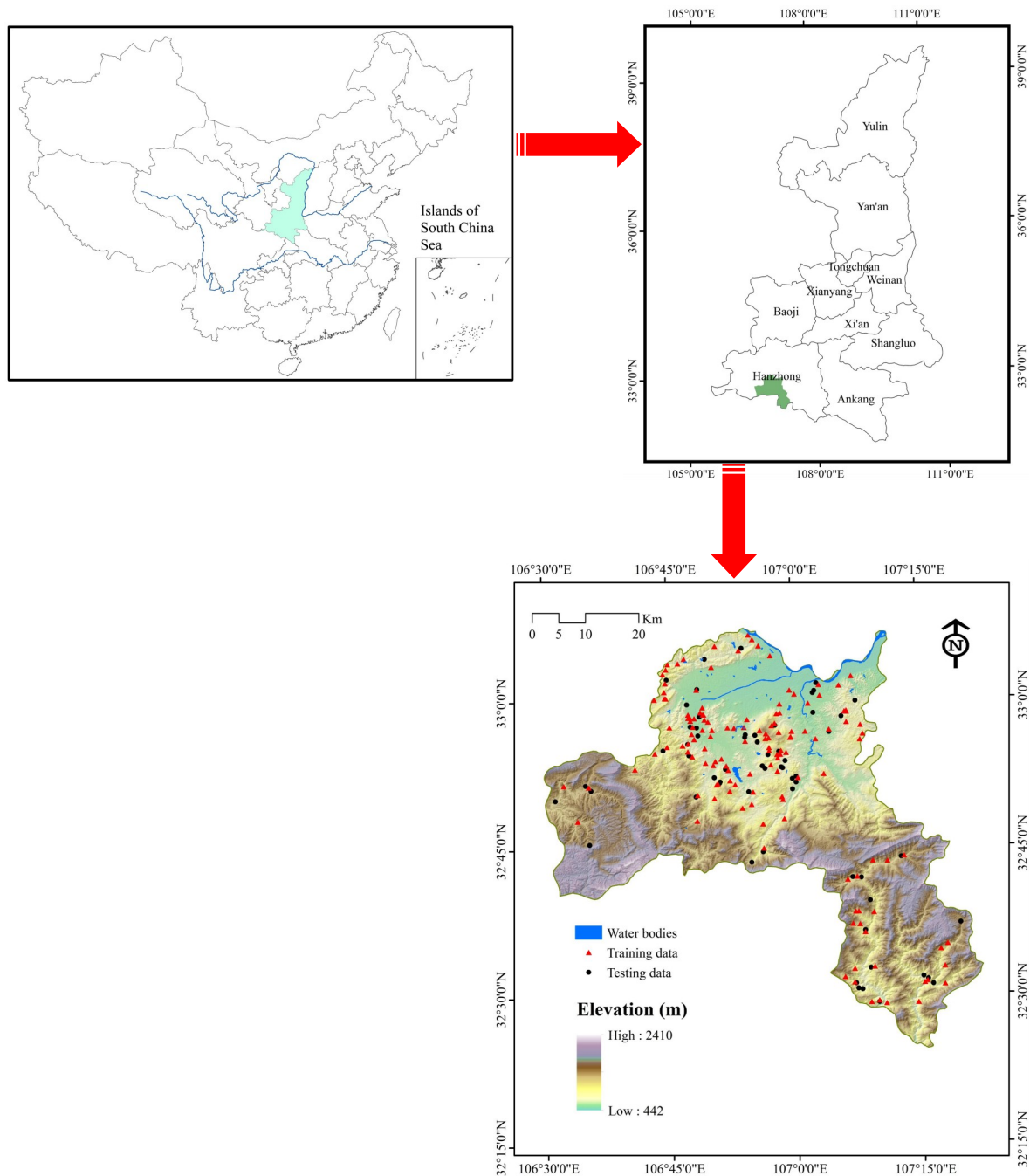


Figure 1. Location of the study area.

Geologically, the study area is located at the northern margin of the Yangtze plate. There are five major faults crossing the area including (1) the Gangchang fault (SW–NE direction), (2) the Xiaolengba–Qinjiaba fault (NW–SE direction), (3) the Xiaoba–Haitang fault (SW–NE direction), (4) the Moujiaba–Shuimohe fault (W–E direction), and (5) the Jiangjiawan–Zhujiaba–Tuqiangping fault (SW–NE direction) (Figure 2).

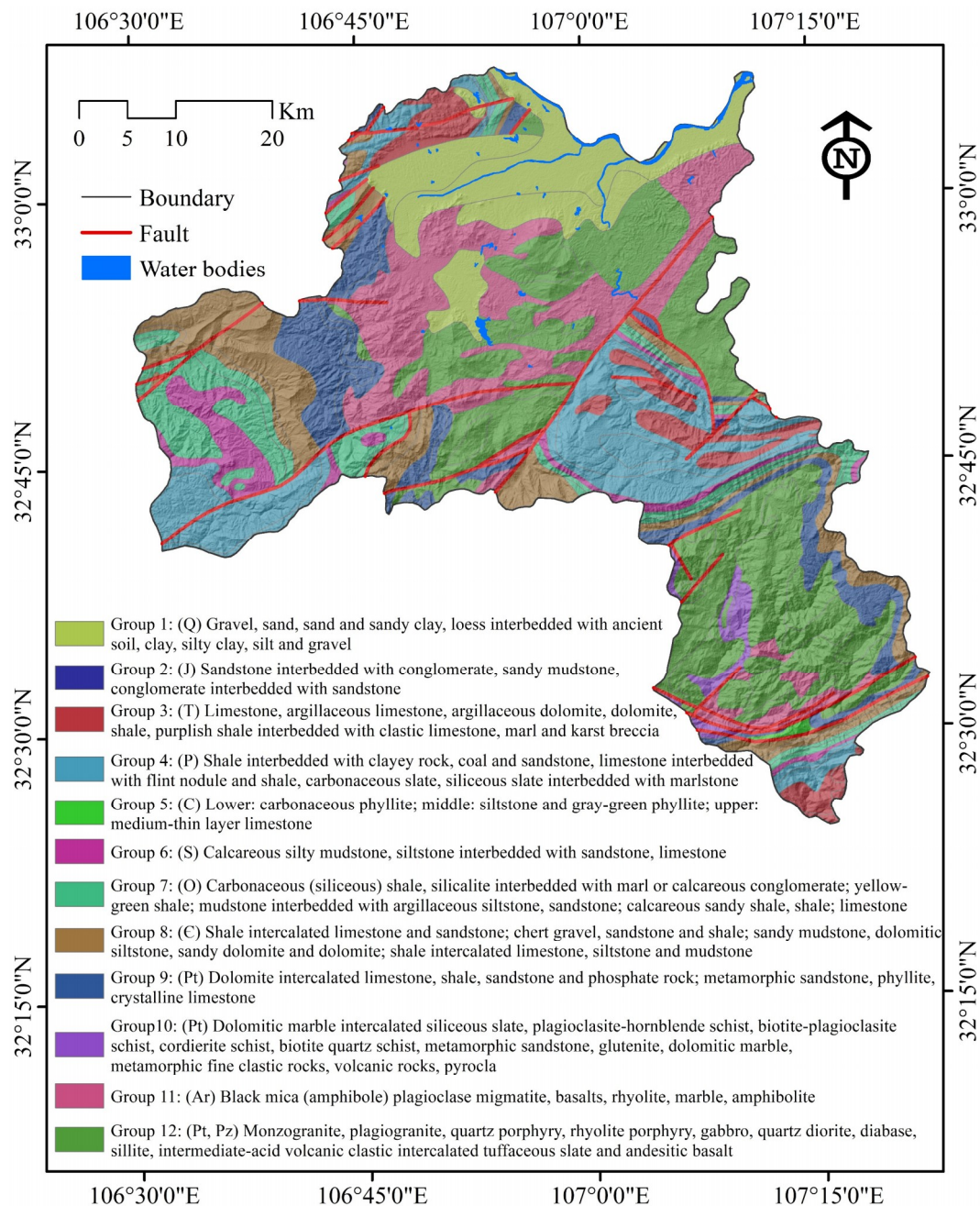


Figure 2. Geological map of the study area.

### 3. Materials and Methods

#### 3.1. Data Preparation

A landslide inventory includes the locations of the past and recent landslides [21]. A landslide inventory can give insight into landslide location, dates, type, frequency of occurrence, state of activity, magnitude or size, failure mechanisms, causal factors, and damage caused [58,59]. In the present study, the landslide inventory map was prepared on the basis of satellite images (Google Earth and ZY03 images) and historical landslide records of the area, which were verified by GPS. A total of 202 landslides were identified to prepare the landslide susceptibility map, of which most of the landslides were slides (190), the others included 12 rock falls [60]. According to an analysis in the GIS environment, the smallest landslide was nearly 160 m<sup>3</sup>, the largest landslide was more than 1,000,000 m<sup>3</sup>, while the average was 33,000 m<sup>3</sup>. Finally, 141 landslides were randomly selected

as training data and rest of them were used for the verification of the landslide susceptibility map (Figure 1).

There are no universal guidelines for selecting landslide conditioning factors [33,61]. A total of 16 landslide conditioning factors were used for landslide susceptibility mapping including slope angle, slope aspect, elevation, plan curvature, profile curvature, topographic wetness index (TWI), stream power index (SPI), sediment transport index (STI), distance to rivers, distance to roads, distance to faults, soil, land use, normalized difference vegetation index (NDVI), lithology, and rainfall, which are considered as controlling factors in the occurrence of landslides in the study area.

Slope angle is an important factor that affects the stress state of slope mass, and these positions where stress exceeds failure strength may contribute to landslide hazards [62,63]. In this case, as shown in Figure 3a, the thematic data layer of the slope angle was reclassified into seven categories with an interval of  $10^\circ$ , namely, (0– $10^\circ$ ), (10– $20^\circ$ ), (20– $30^\circ$ ), (30– $40^\circ$ ), (40– $50^\circ$ ), (50– $60^\circ$ ), and (60– $72.83^\circ$ ).

Slope aspect is another common conditioning factor for the task of landslide susceptibility mapping [64,65]. It has been proven that most landslides usually occur at a certain slope aspect for a given study area, but the mechanism has not been revealed clearly [66]. Therefore, slope aspect was also employed as a conditioning factor. Here, slope aspect categories include flat, north, northeast, east, southeast, south, southwest, west, and northwest (Figure 3b).

Generally, it is considered that elevation has a firm relationship with landslide occurrence [67]. There is no denying that elevation can influence the topography, vegetation, temperature, humidity, human activities, and many other conditions that have a connection with slope stability [30,68]. In Figure 3c, the elevation of the study area was divided into ten classes with an interval of 200 m, i.e., (442–600 m), (600–800 m), (800–1000 m), (1000–1200 m), (1200–1400 m), (1400–1600 m), (1600–1800 m), (1800–2000 m), (2000–2200 m), and (2200–2410 m).

Plan curvature and profile curvature are two quantitative indices that embody topographic characteristics and trend from different perspectives [69]. Various curvature values indicate different runoff and erosion conditions of water. For instance, the upwardly convex surfaces have positive curvature values while negative curvature values mean upwardly concave surfaces [30]. In this study, the plan curvature and profile curvature values were both reclassified into three groups (Figure 3d,e).

TWI was proposed to indicate the local groundwater potential by Moore [70] in 1991. Currently, TWI is regarded as an extensively-used causative factor in landslide susceptibility assessment [71]. It is expressed as  $TWI = \ln\left(\frac{\alpha}{\tan \beta}\right)$ , where  $\beta$  is the slope angle (radian), and  $\alpha$  is the flow accumulation through a point [72]. The TWI values of the study area can be calculated by GIS software and reclassified as (<4), (4–5), (5–6), (6–7), and (>7) with an interval of 1 (Figure 3f).

SPI can directly measure the erosion capacity of the stream. A higher SPI value indicates that the stream has more powerful erosion on the slope surface [55]. The SPI values are mainly determined as  $SPI = \alpha \tan \beta$  [54,70]. In this study, the SPI values were identified as five categories with an interval of 20, namely, (<20), (20–40), (40–60), (60–80), and (>80) (Figure 3g).

As another topographic index, STI has also been considered to construct the landslide susceptibility model [73]. Similar to SPI, STI can quantitatively reflect the regional topographic features and erosion conditions [74]. For the present study, STI values contained five categories with an interval of 10: (<10), (10–20), (20–30), (30–40), (>40) (Figure 3h).

Rivers can not only affect the moisture distribution in slopes, but can also erode the toes of slopes, which cause slope deformation and failure [75]. Thus, it is necessary to consider the river effects when producing landslide susceptibility maps. In this study, based on the distance to rivers, five buffer zones with an interval of 200 m were generated for each river: (<200 m), (200–400 m), (400–600 m), (600–800 m), and (>800 m) (Figure 3i).

Generally speaking, road construction in mountainous areas, which always produce an engineering load and destroy the integrity of slope structure, have significant negative impacts on the slope stability [76]. Hence, the distance to roads is usually selected as a conditioning factor to embody the influence of road engineering activities on landslide occurrence [77]. Here, values of the

distance to roads were divided into five groups with an interval of 300 m, i.e., (<300 m), (300–600 m), (600–900 m), (900–1200 m), and (>1200 m) (Figure 3j).

Fault structures affect the spatial distribution and characteristics of landslides in a certain region [50]. According to relevant studies [30,78], the integrity of rock and soil mass generally decrease as the distance to the faults shorten. In this way, landslide hazards are more likely to occur in the neighboring area of faults. Ultimately, buffers of various faults in the study area were obtained and reclassified into five categories with an interval of 1000 m: (<1000 m), (1000–2000 m), (2000–3000 m), (3000–4000 m), and (>4000 m) (Figure 3k).

In terms of soil, this is an essential factor that has a strong correlation with landslide occurrence [79]. To a great extent, the strength, root cohesion, permeability, and vegetation coverage of the soil mass depend on the soil type [80,81], which can impact the failure characteristics of slopes [82,83]. In this study area, a total of nine soil types were identified including cumulic anthrosol, dystric cambisol, eutric cambisol, calcareous fluvisol, haplic luvisol, chromic luvisol, eutric planosol, calcareous regosol, and eutric regosol (Figure 3l).

Land use is one of the most frequently used conditioning factors, and the correlation between landslides and land use has been confirmed [84]. For instance, in some farmland regions, landslides are frequent and common under long-term irrigation [85]. For the study area, the types of land use mainly consist of farmland, forestland, grassland, water, residential areas, and bareland (Figure 3m).

NDVI is a very popular index to measure the degree of vegetation in a region. NDVI values can be figured out by the formula  $NDVI = (I - R) / (IR + R)$ , where IR is the infrared band and R is the red band of the electromagnetic spectrum [86]. The range of NDVI values is from  $-1$  to  $1$ , and a positive value means that the local ground is covered by vegetation. Five categories of NDVI values were generated based on the natural break method [87], namely ( $-0.21-0.21$ ), ( $0.21-0.36$ ), ( $0.36-0.44$ ), ( $0.44-0.52$ ), and ( $0.52-0.65$ ) (Figure 3n).

Like soil, lithology is one of the most important factors that directly determines slope stability. According to many existing studies, the physical and mechanical properties of rock mass usually change dramatically with lithological units [88]. Therefore, most landslides occur in the sliding-prone lithological units that have lower strength and a higher moisture content. For this study area, the strata were mainly reclassified into twelve lithological units based on the lithofacies and geological ages, and the specific distribution of various lithologies was illustrated in Figure 3o.

Rainfall is a crucial triggering factor that causes massive landslides by means of raising the groundwater level and increasing pore water pressure [89]. It can be observed that the probability of landslide occurrence indeed grows under the actions of long-term or heavy rainfall. Based on the meteorological data of the study area, the corresponding rainfall map with an interval of 100 mm/yr was produced, i.e., (<900 mm/yr), (900–1000 mm/yr), (1000–1100 mm/yr), (1100–1200 mm/yr), (1200–1300 mm/yr), (1300–1400 mm/yr), (1400–1500 mm/yr), (1500–1600 mm/yr), (1600–1700 mm/yr), and (>1700 mm/yr) (Figure 3p).

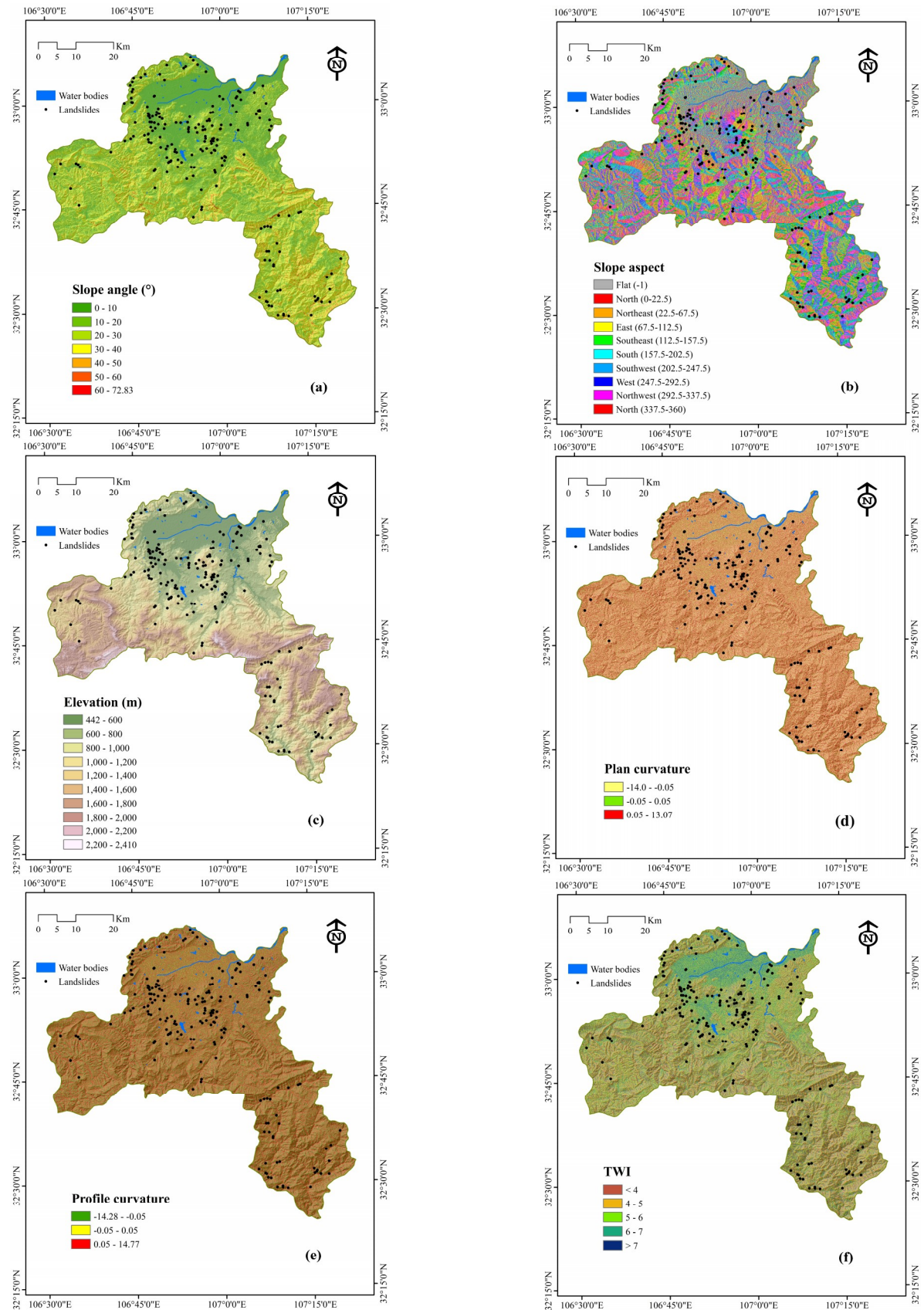


Figure 3. Cont.

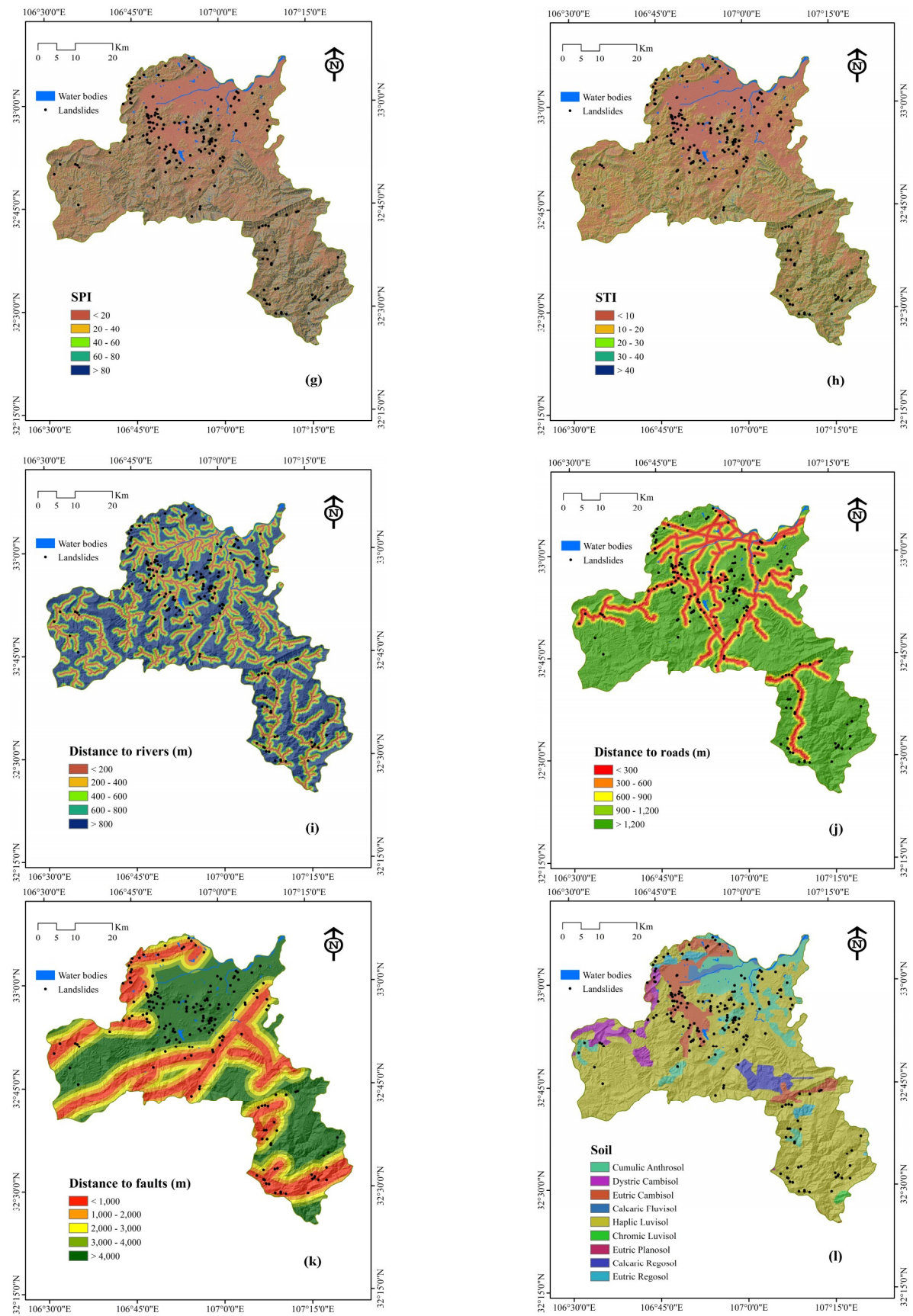
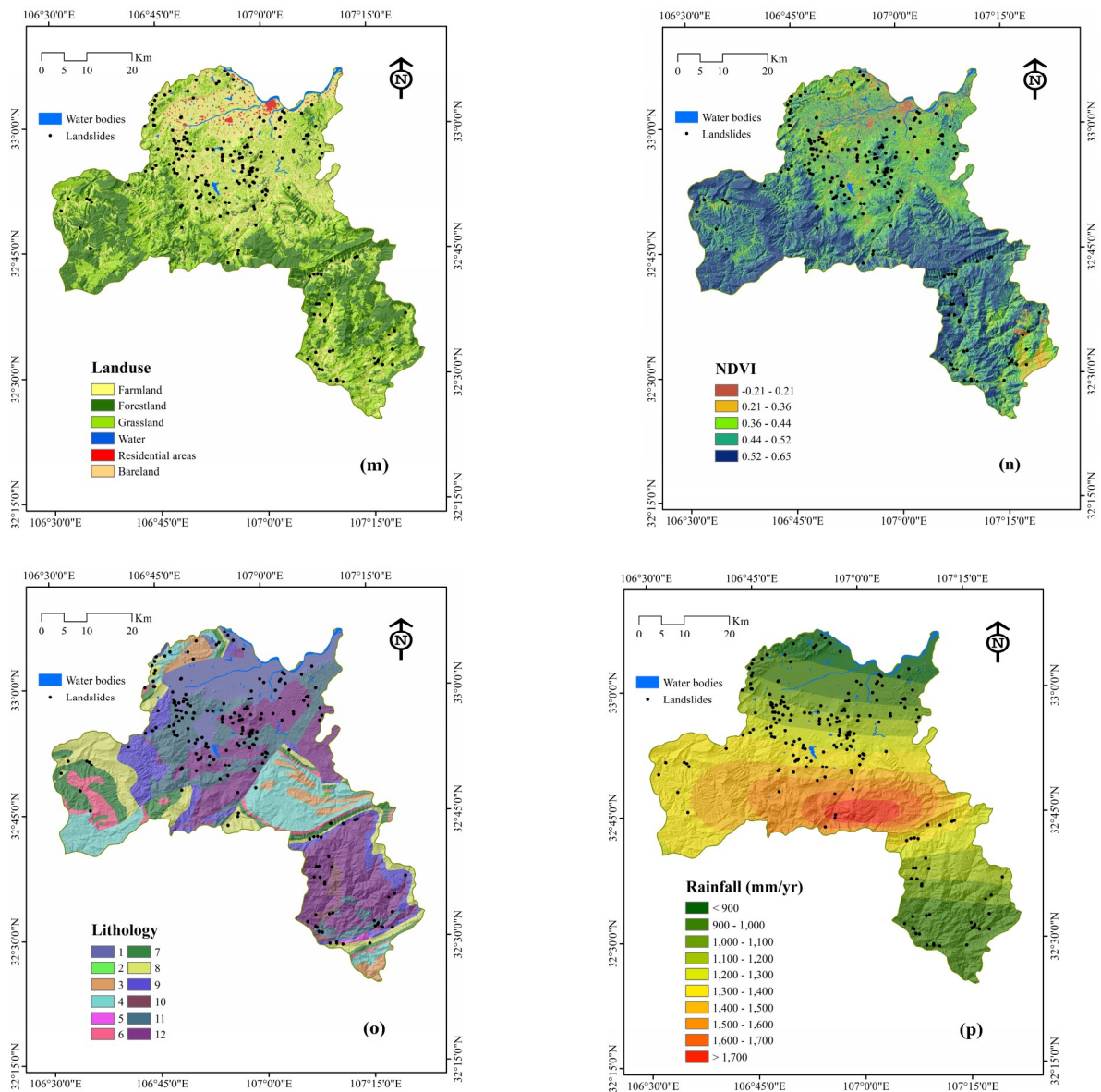


Figure 3. Cont.



**Figure 3.** Thematic maps: (a) Slope angle; (b) Slope aspect; (c) Elevation; (d) Plan curvature; (e) Profile curvature; (f) TWI; (g) SPI; (h) STI; (i) Distance to rivers; (j) Distance to roads; (k) Distance to faults; (l) Soil; (m) Land use; (n) NDVI; (o) Lithology; and (p) Rainfall.

### 3.2. Weight of Evidence

Weight of evidence (WoE) is one of the most popular models that uses the Bayesian theory of conditional probability to quantify spatial associations between evidence layers and known mineral occurrences [90]. In the WoE method, conditional independence is the most important issue that should be considered. The WoE is based on the calculation of positive weight  $W^+$  and negative weight  $W^-$  as follows:

$$W^+ = \ln \frac{p\{B|A\}}{p\{B|\bar{A}\}} \tag{1}$$

$$W^- = \ln \frac{p\{\bar{B}|A\}}{p\{\bar{B}|\bar{A}\}} \tag{2}$$

where  $B$  is the presence predictive factor;  $\bar{B}$  is the absence of the predictive factor;  $A$  is the presence of landslide; and  $\bar{A}$  is the absence of landslide. In landslide susceptibility prediction, the weight

contrast  $W_f = W^+ - W^-$  was used to measure and reflect the spatial association between the landslide conditioning factors and landslide occurrence [91].

### 3.3. Logistic Regression

Logistic regression (LR) is one type of regression analysis where categorical outcomes can be predicted based on a certain predictor [92]. By using the logistic functions, probabilities of the possible outcomes can be modeled [93].

The logistic regression model is useful for two-class classification. Assuming there are  $n$  samples of the pairs,  $(x_i, y_i)$ ,  $i = 1, 2, \dots, n$ ,  $y_i \in \{-1, +1\}$  is a binary class label for each sample  $i = 1, 2, \dots, n$  and weights  $(w, b)$ . In the logistic regression for binary classification, the occurrence probability of the class is modeled with the below function:

$$P(y = \pm 1|x, w) = \frac{1}{1 + \exp(-y(w^T x + b))} \quad (3)$$

where  $b$  is the intercept;  $T$  is the matrix transposition; and the  $k$ -dimensional coefficient vector,  $w = (w_1, w_2, \dots, w_k)^T$  are parameters to be estimated.

### 3.4. Random Forest

Random forests (RF) are an ensemble of separately trained binary decision trees [94]. In the random forest algorithm, a random vector  $i_k$  is naturally produced, independent from the previous random vectors and distributed to all trees, and each tree is grown using the training dataset and random vector  $i_k$ , and outcomes are in the collection of tree-structured classifiers  $h(x, i_k)$ ,  $k = 1, 2, \dots, n$  at input vector  $x$ . In this study,  $i_k$  is the landslide conditioning factors. The random forest consisted of two trees, namely, landslide and non-landslide, each constructed while considering sixteen random features.

Generally, in a random forest algorithm, the generalization error is described as below [95]:

$$GE = P_{x,y}(mg(x, y) < 0) \quad (4)$$

where  $x$  and  $y$  are the landslide conditioning factors indicating the probability over the  $x, y$  space, and  $mg$  is the margin function, which is defined as below:

$$mg(x, y) = av_k I(h_k(x) = y) - \max_{j \neq y} av_k I(h_k(x) = j) \quad (5)$$

Which measures the extent to which the average number of votes at random vectors for the right output exceeds the average vote for any other output. The  $I(*)$  is the indicator function [96].

## 4. Results

### 4.1. Correlation Analysis

The correlation between the conditioning factors and probability of landslides occurrence was measured by the weight contrast  $W_f$ , and the calculation results of the WoE model are listed in Table 1. The LR method was employed to produce the landslide susceptibility map, and one of the most critical applicable conditions of LR is that the landslide conditioning factors are mutually independent [97]. Therefore, it is necessary to diagnose the multicollinearity of various conditioning factors when evaluating landslide susceptibility [98]. Currently, the tolerance (TOL) ( $TOL = 1 - R^2$ , and  $R$  is the coefficient of determination of the regression equation) and variance inflation factor (VIF) ( $VIF = 1/TOL$ ) have been applied in multicollinearity diagnosis [99–101].

**Table 1.** Correlation between landslides and conditioning factors using the WoE model.

Factors	Class	No. of Landslide	No. of Pixels in Domain	W <sup>+</sup>	W <sup>-</sup>	W <sub>f</sub>
Slope angle (°)	0–10	36	738,360	0.077	−0.025	0.102
	10–20	63	914,163	0.423	−0.246	0.669
	20–30	29	821,142	−0.246	0.075	−0.320
	30–40	11	468,077	−0.653	0.081	−0.734
	40–50	2	155,377	−1.255	0.037	−1.292
	50–60	0	24,357	0.000	0.008	0.000
	60–72.83	0	1710	0.000	0.001	0.000
Slope aspect	Flat	0	874	0.000	0.000	0.000
	North	16	443,863	−0.225	0.033	−0.258
	Northeast	16	405,251	−0.134	0.019	−0.153
	East	17	376,207	0.001	0.000	0.001
	Southeast	23	390,547	0.266	−0.044	0.310
	South	32	374,222	0.639	−0.130	0.769
	Southwest	13	344,928	−0.181	0.020	−0.201
	West	9	354,647	−0.576	0.055	−0.631
	Northwest	15	432,647	−0.264	0.037	−0.301
Elevation (m)	442–600	28	413,571	0.405	−0.079	0.485
	600–800	48	512,157	0.730	−0.237	0.968
	800–1000	31	377,619	0.598	−0.119	0.717
	1000–1200	17	326,381	0.143	−0.018	0.161
	1200–1400	15	398,407	−0.182	0.024	−0.206
	1400–1600	2	385,439	−2.163	0.117	−2.281
	1600–1800	0	376,083	0.000	0.128	0.000
	1800–2000	0	247,350	0.000	0.083	0.000
	2000–2200	0	78,216	0.000	0.025	0.000
	2200–2410	0	7963	0.000	0.003	0.000
Plan curvature	−14.0– −0.05	58	144,0116	−0.114	0.088	−0.203
	−0.05–0.05	13	215,290	0.291	−0.025	0.316
	0.05–13.07	70	1,467,780	0.055	−0.051	0.106
Profile curvature	−14.28– −0.05	66	1,428,952	0.023	−0.020	0.042
	−0.05–0.05	16	177,891	0.689	−0.062	0.751
	0.05–14.77	59	1,516,343	−0.149	0.123	−0.271
TWI	<4	11	558,428	−0.829	0.116	−0.945
	4–5	50	1,000,955	0.101	−0.052	0.153
	5–6	48	746,522	0.354	−0.143	0.497
	6–7	20	393,490	0.119	−0.018	0.137
	>7	12	423,791	−0.467	0.057	−0.523
SPI	<20	88	1,740,663	0.113	−0.164	0.277
	20–40	20	497,521	−0.116	0.021	−0.137
	40–60	12	231,236	0.139	−0.012	0.151
	60–80	5	133,800	−0.189	0.008	−0.197
	>80	16	519,966	−0.383	0.062	−0.445
STI	<10	90	1,722,652	0.146	−0.215	0.361
	10–20	32	702,426	0.009	−0.003	0.012
	20–30	6	295,062	−0.798	0.056	−0.853
	30–40	5	141,300	−0.244	0.010	−0.254
	>40	8	261,746	−0.390	0.029	−0.419
Distance to rivers (m)	<200	27	521,129	0.138	−0.030	0.168
	200–400	22	463,390	0.050	−0.009	0.059
	400–600	18	427,717	−0.070	0.011	−0.081
	600–800	19	374,831	0.116	−0.017	0.133
	>800	55	1,336,119	−0.092	0.064	−0.156
Distance to roads (m)	<300	33	343,852	0.754	−0.150	0.904
	300–600	16	279,559	0.237	−0.027	0.264
	600–900	8	245,226	−0.325	0.023	−0.348
	900–1200	15	219,752	0.413	−0.040	0.453
	>1200	69	2,034,797	−0.286	0.382	−0.668

Table 1. Cont.

Factors	Class	No. of Landslide	No. of Pixels in Domain	W <sup>+</sup>	W <sup>-</sup>	W <sub>f</sub>
Distance to faults (m)	<1000	32	671,796	0.054	-0.015	0.069
	1000–2000	18	503,008	-0.232	0.039	-0.271
	2000–3000	21	412,189	0.121	-0.020	0.141
	3000–4000	8	348,794	-0.677	0.060	-0.737
	>4000	62	1,187,399	0.145	-0.101	0.246
Soil	Cumulic Anthrosol	20	360,361	0.206	-0.030	0.237
	Dystric Cambisol	4	113,893	-0.251	0.008	-0.259
	Eutric Cambisol	31	249,592	1.012	-0.165	1.177
	Calcaric Fluvisol	0	37,035	0.000	0.012	0.000
	Haplic Luvisol	80	2,211,459	-0.222	0.393	-0.615
	Chromic Luvisol	0	10,045	0.000	0.003	0.000
	Eutric Planosol	3	14,836	1.500	-0.017	1.516
	Calcaric Regosol	1	82,141	-1.311	0.020	-1.330
	Eutric Regosol	2	43,824	0.011	0.000	0.011
	Land use	Farmland	86	90,0284	0.750	-0.601
Forestland		4	96,7369	-2.390	0.342	-2.732
Grassland		51	1,202,442	-0.062	0.037	-0.100
Water		0	18,838	0.000	0.006	0.000
Residential areas		0	33,563	0.000	0.011	0.000
Bareland		0	690	0.000	0.000	0.000
NDVI	-0.21–0.21	4	67,502	0.272	-0.007	0.279
	0.21–0.36	10	207,991	0.063	-0.005	0.068
	0.36–0.44	63	651,020	0.762	-0.358	1.121
	0.44–0.52	56	1,089,392	0.130	-0.077	0.207
	0.52–0.65	8	1,107,281	-1.832	0.379	-2.212
Lithology	1	27	363,139	0.499	-0.089	0.588
	2	0	1694	0.000	0.001	0.000
	3	2	136,901	-1.128	0.031	-1.159
	4	6	398,403	-1.098	0.093	-1.191
	5	0	7470	0.000	0.002	0.000
	6	0	107,848	0.000	0.035	0.000
	7	5	225,834	-0.713	0.039	-0.751
	8	10	319,450	-0.366	0.034	-0.401
	9	9	276,290	-0.326	0.027	-0.353
	10	1	39,158	-0.570	0.005	-0.575
	11	32	435,539	0.487	-0.107	0.594
	12	49	811,460	0.291	-0.126	0.417
Rainfall (mm/yr)	<900	8	189,533	-0.067	0.004	-0.071
	900–1000	29	582,217	0.098	-0.024	0.122
	1000–1100	23	282,006	0.591	-0.083	0.675
	1100–1200	35	329,319	0.856	-0.174	1.030
	1200–1300	16	271,086	0.268	-0.030	0.298
	1300–1400	18	629,601	-0.457	0.089	-0.545
	1400–1500	7	351,254	-0.818	0.068	-0.886
	1500–1600	3	270,784	-1.405	0.069	-1.474
	1600–1700	1	135,625	-1.812	0.037	-1.849
>1700	1	81,761	-1.306	0.019	-1.325	

Generally, a TOL value less than 0.1 or a VIF value larger than 10 is regarded as a symbol of multicollinearity [61]. In this study, the results of the WoE model were used as inputs to calculate the TOL and VIF values of all of the conditioning factors. In accordance with the calculated results, there was no multicollinearity among the landslide conditioning factors (Table 2).

**Table 2.** Multicollinearity analysis.

Landslide Conditioning Factors	Collinearity Statistics	
	Tolerance (TOL)	Variance inflation factors (VIF)
Slope angle	0.761	1.315
Slope aspect	0.883	1.133
Elevation	0.650	1.539
Plan curvature	0.714	1.400
Profile curvature	0.855	1.170
TWI	0.828	1.208
SPI	0.434	2.303
STI	0.402	2.489
Distance to rivers	0.946	1.057
Distance to roads	0.779	1.284
Distance to faults	0.908	1.101
NDVI	0.774	1.292
Soil	0.642	1.557
Land use	0.627	1.595
Lithology	0.765	1.308
Rainfall	0.664	1.507

#### 4.2. Application of the WoE Model

In terms of slope angle, the slope angle between 10°–20° (0.669) is more prone to landslide occurrence. Additionally, the  $W_f$  values of the region where slope angles larger than 50° are 0. For the slope aspect factor,  $W_f$  was the highest for south-facing (0.769). Furthermore, southeast-facing (0.310) and east-facing (0.001) also had a positive correlation with landslide occurrence. In the case of elevation, most landslides were distributed in the classes of 442–600 m (0.485), 600–800 m (0.968), and 800–1000 m (0.717). When the elevation was larger than 1200 m, elevation had an inhibitory effect on landslides. In the case of plan curvature, flat areas had a more important impact on landslides, whereas the  $W_f$  values of convex areas and concave areas were 0.106 and  $-0.203$ , respectively. In the case of profile curvature, the  $W_f$  values of the concave class, flat class, and convex class were 0.042, 0.751, and  $-0.271$ , respectively. For TWI, the highest  $W_f$  value was observed for the interval of 5–6 (0.497) while the class  $<4$  ( $-0.945$ ) had the lowest value. For SPI, the class  $<20$  (0.277) had the highest  $W_f$  value, and the areas of SPI 20–40 and  $>60$  were negative for landslides. For STI, the class  $<10$  had the highest  $W_f$  value of 0.361, while the class 20–30 had the lowest value of  $-0.853$ . In the case of distance to rivers, the classes of  $<200$  m (0.168) and 600–800 m (0.133) occupied higher  $W_f$  values when compared to the other classes. In the case of distance to roads, the class of  $<300$  m (0.904) had a more intimate correlation with landslide occurrence. In the case of distance to faults, it can be seen that the class  $>4000$  m had the highest  $W_f$  value of 0.246. For soil, eutric cambisol (1.177) and eutric planosol (1.516) were more likely to induce landslides due to the dramatic falling of soil strength under saturated conditions [85]. For land use, farmland (1.351) had the highest probability of landslide occurrence, which may be essentially caused by irrigation. According to the  $W_f$  values of NDVI, the class of 0.36–0.44 (1.121) mainly contributed to landslide occurrence, while the lowest value was for the class of 0.52–0.65 ( $-2.212$ ), which indicates that high vegetation coverage can restrain landslides. In the case of lithology, the  $W_f$  values of group 1 (Q) (0.588), group 11 (Ar) (0.594), and group 12 (Pt, Pz) (0.417) were larger than 0, indicating that these lithological groups had the highest susceptibility to landslide. In the case of rainfall, the range between 1100–1200 mm/yr (1.030) showed high susceptibility for landslide occurrence.

The calculated  $W_f$  values for all landslide conditioning factors were summed using the following equation to construct the landslide susceptibility map (LSM):

$$\begin{aligned}
 LSM_{WoE} = & \text{Slope angle}_{Wf} + \text{Slope aspect}_{Wf} + \text{Elevation}_{Wf} + \text{Plan curvature}_{Wf} \\
 & + \text{Profile curvature}_{Wf} + \text{TWI}_{Wf} + \text{SPI}_{Wf} + \text{STI}_{Wf} + \text{Distance to rivers}_{Wf} \\
 & + \text{Distance to roads}_{Wf} + \text{Distance to faults}_{Wf} + \text{NDVI}_{Wf} + \text{Soil}_{Wf} + \text{Landuse}_{Wf} \\
 & + \text{Lithology}_{Wf} + \text{Rainfall}_{Wf}
 \end{aligned}
 \tag{6}$$

The integrated result of the WoE model is shown in Figure 4. The LSM was reclassified into five classes based on the natural break method: very low, low, moderate, high, and very high.

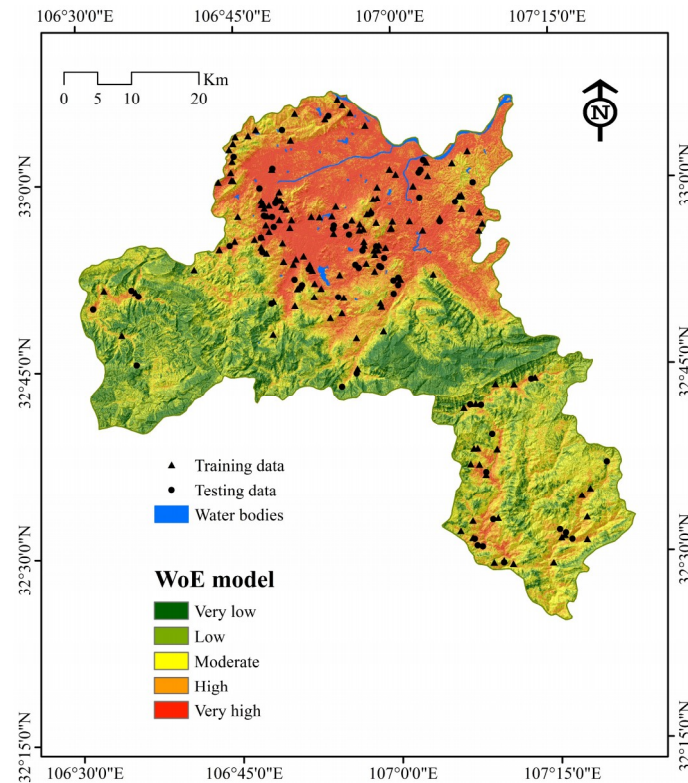


Figure 4. Landslide susceptibility map using the WoE model.

### 4.3. Application of the WoE-LR Model

In this case, SPSS 18.0 software was applied to build a landslide susceptibility model with the WoE-LR model. The input table of the LR model can be generated by the determined class values of variables based on the WoE model [54]. In the analysis process, a forward stepwise LR was adopted, and the analysis results are given in Tables 3 and 4. The Cox and Snell R Square (0.245) and Nagelkerke R Square (0.326) are two pseudo determined coefficients that are used to reflect the degree of independent variables explaining dependent variables [102,103]. According to Table 4, the LR equation and landslide occurrence probability  $P$  can be expressed as Equations (7) and (8), respectively.

$$\begin{aligned}
 y = & 1.122 \times \text{Slope angle} + 2.157 \times \text{Slope aspect} + 0.986 \times \text{Elevation} \\
 & + 2.505 \times \text{Plan curvature} + 0.868 \times \text{Profile curvature} + 1.764 \times \text{TWI} \\
 & + 1.427 \times \text{SPI} + 1.142 \times \text{STI} + 0.512 \times \text{Distance to rivers} \\
 & + 1.445 \times \text{Distance to roads} + 0.972 \times \text{Distance to faults} \\
 & + 0.859 \times \text{NDVI} + 1.392 \times \text{Soil} + 1.634 \times \text{Landuse} + 1.032 \times \text{Lithology} \\
 & + 1.594 \times \text{Rainfall} + 0.806
 \end{aligned}
 \tag{7}$$

$$P = \frac{e^y}{1 + e^y}
 \tag{8}$$

**Table 3.** Maximum likelihood estimation and Cox and Snell’s and Nagelkerke’s R-square.

−2 Log Likelihood	Cox & Snell R Square	Nagelkerke R Square
311.780	0.245	0.326

**Table 4.** Coefficients of WoE-LR model.

Landslide Conditioning Factors	Coefficients
Slope angle	1.122
Slope aspect	2.157
Elevation	0.986
Plan curvature	2.505
Profile curvature	0.868
TWI	1.764
SPI	1.427
STI	1.142
Distance to rivers	0.512
Distance to roads	1.445
Distance to faults	0.972
NDVI	0.859
Soil	1.392
Land use	1.634
Lithology	1.032
Rainfall	1.594
Constant	0.806

Ultimately, the landslide susceptibility index (LSI) for the LR model were obtained based on Equation (8), moreover, the LSI values were reclassified into five categories by the natural break method: very low, low, moderate, high, and very high (Figure 5).

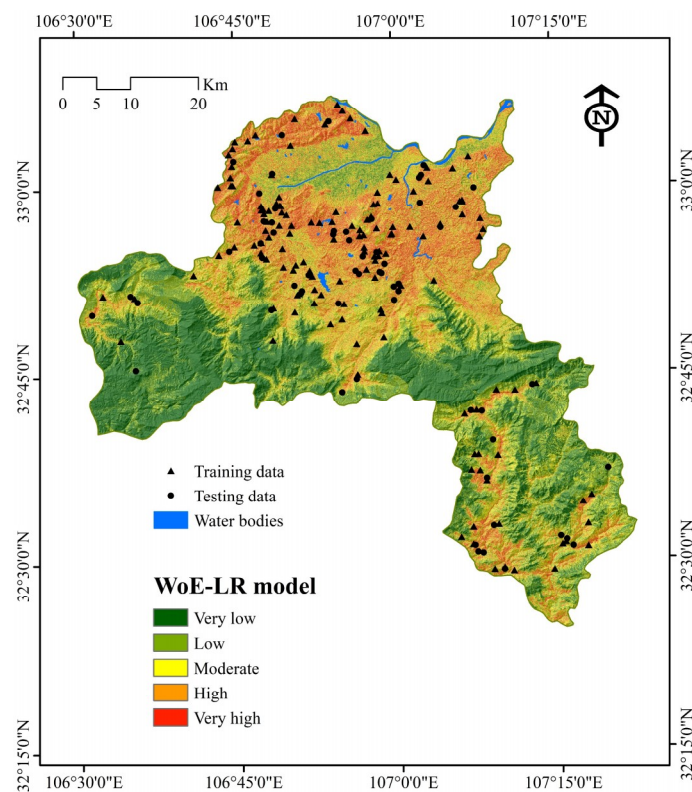


**Figure 5.** Landslide susceptibility map using the WoE-LR model.

#### 4.4. Application of the WoE-RF Model

Similarly, the calculated results of the WoE model can be used as input for the RF model. In this study, training of the RF model was implemented by WEKA software. During the analyzing process, the importance of various conditioning factors can be measured quantitatively and ordered by MDA (mean decrease accuracy) and MDG (mean decrease Gini). Generally, MDA is determined during the Out-Of-Bag error calculation phase, while MDG is a measure of how each variable contributes to the homogeneity of the nodes and leaves [104]. The values of the above-mentioned two metrics of the conditioning factors are illustrated in Figure 6, and a larger value of MDA or MDG means a higher importance of the corresponding variable. Accordingly, in terms of MDA, land use is the most critical factor in the RF model, while soil is second in importance only to land use. For the MDG, the importance of elevation was first, followed by rainfall and land use. Finally, based on ArcGIS software, the landslide susceptibility map using the WoE-RF was generated and is shown in Figure 7.

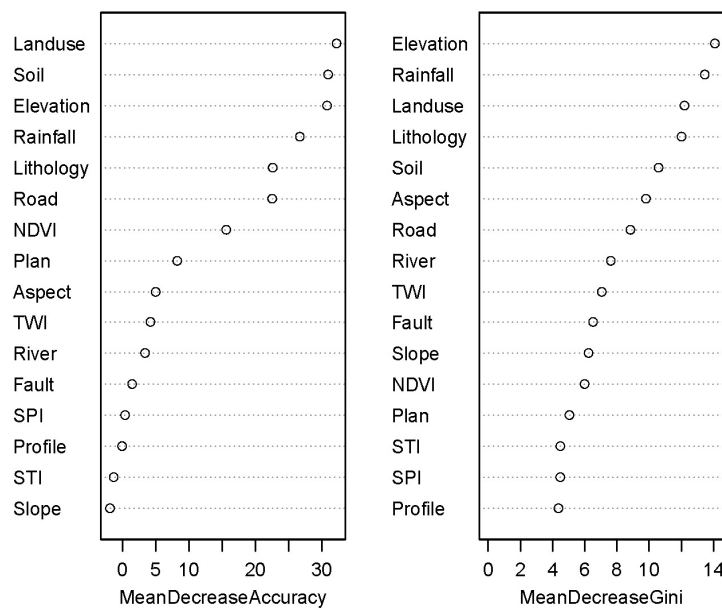


Figure 6. Mean decrease accuracy and mean decrease Gini.

#### 4.5. Validation of Landslide Models

Currently, the ROC and AUC have been widely applied to validate the performance of determined landslide susceptibility models [64,69,105]. The ROC curve can be generated by plotting the false positive rate (100-specificity) in the x-axis versus the sensitivity in the y-axis [71]. The area under the ROC curve (AUC) is an indicator of the global summary measure of the performance of a model [106–108]. In the present study, to assess the validation of the WoE, WoE-LR, and WoE-RF models, the ROC curves of three models with training and validation datasets are described in Figures 8 and 9.

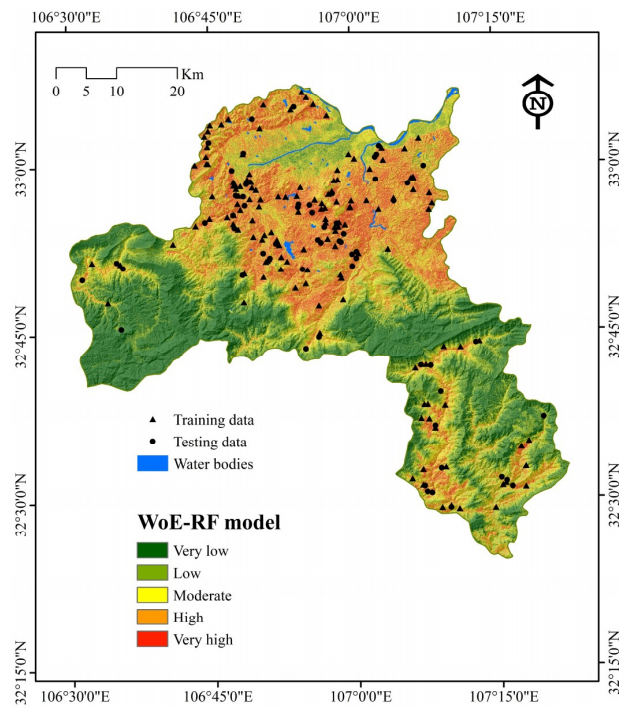


Figure 7. Landslide susceptibility map using the WoE-RF model.

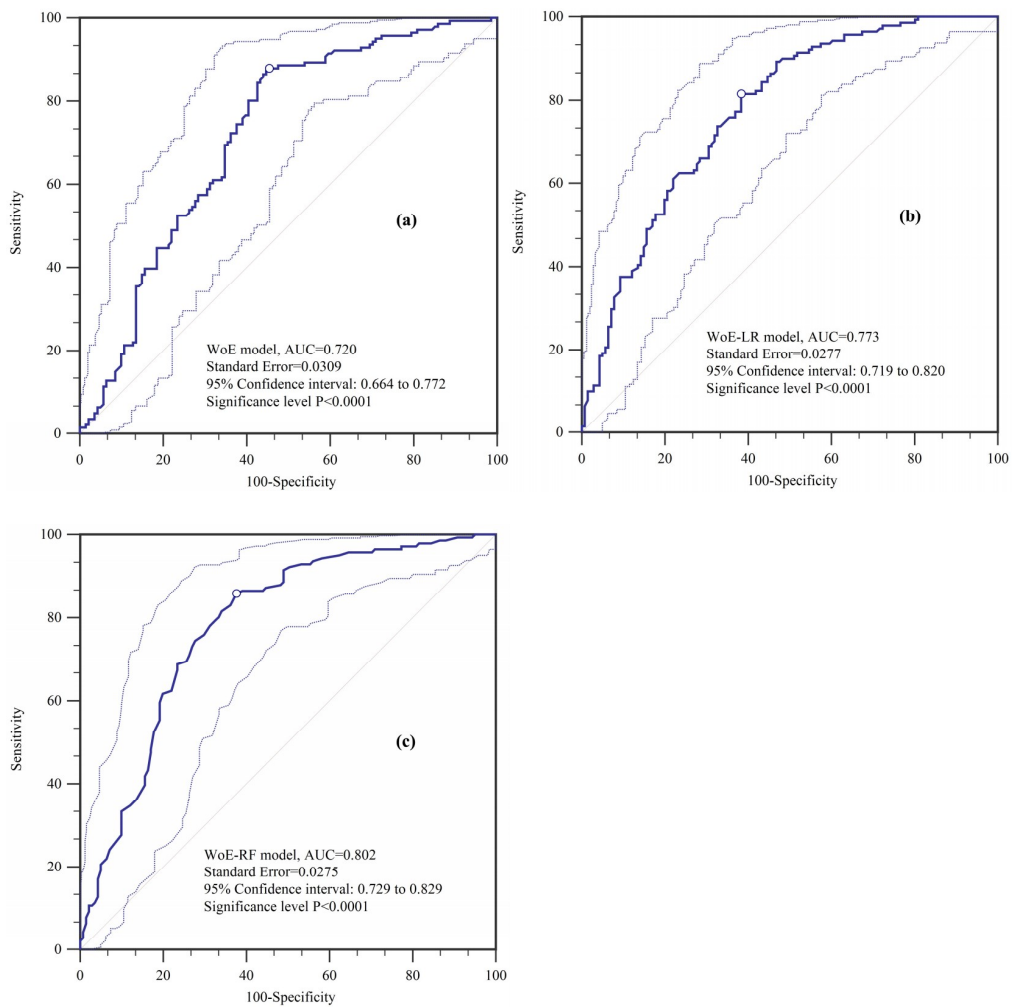
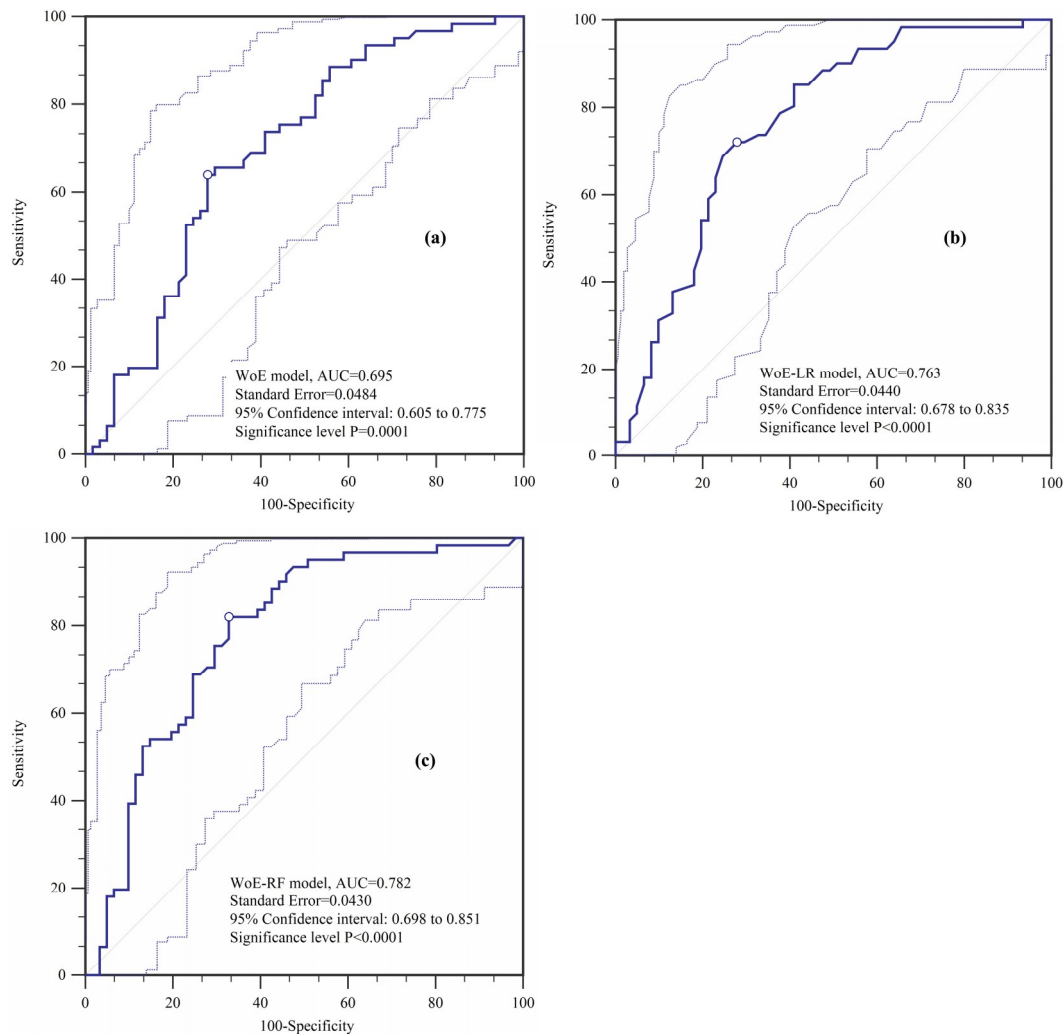


Figure 8. ROC curves using the training dataset.



**Figure 9.** ROC curves using the validation dataset.

In the case of the training dataset, the WoE-RF model had the best performance with the highest AUC value of 0.802, while the AUC values of the WoE model and WoE-LR model were 0.720 and 0.773, respectively. Meanwhile, the WoE-RF model had the lowest standard error (0.0275) and a 95% confidence interval of 0.729–0.829. Thus, the WoE-RF and WoE-LR models can improve the accuracy of the traditional WoE model in this study, and the WoE-RF model showed a relatively better performance.

In the case of the validation data, it can be seen that the AUC values of the various models decreased slightly when compared with the training dataset. The AUC values were 0.695, 0.763, and 0.782 for the WoE model, WoE-LR model, and WoE-RF model, respectively. Similarly, the lowest standard error was 0.0430 for the WoE-RF model, followed by the WoE-LR model (0.0440), and the WoE model (0.0484). The detailed results demonstrated that the WoE-RF model had a prominent prediction capacity on landslide susceptibility mapping.

## 5. Discussions

Under the action of environmental factors and human activities, the frequency of landslide occurrence has been increasing in recent decades, which may result in catastrophic losses on lives, resources, and property [109,110]. Currently, numerous approaches have been used in landslide susceptibility mapping such as FR [23], WoE [19], IoE [111], machine learning [64,112], and ensemble learning models [53,54]. In the above-mentioned models, the probabilistic meaning and calculation procedure of the WoE model are relatively concise and specific, which makes the WoE a classical and

widely used method in landslide susceptibility mapping. Nevertheless, due to the uncertainties and fuzziness in the data of the conditioning factors [113], for different datasets, the performance of the WoE models were significantly distinguished [114–116]. In the present study, the integrated ensemble WoE with LR and RF models were proposed and applied for landslide susceptibility modeling in order to improve the accuracy and generalization ability of the traditional WoE model.

Landslide inventory map is a preliminary step toward landslide susceptibility, hazard and risk assessment [59]. Generally, there are two classes of Landslide inventories: landslide-event inventories that are associated with a trigger and historical landslide inventories [59,117]. In the present study, we adopted the latter formation, which was the sum of many landslide events over a long time. However, the evidence of many smaller landslides might have been lost due to various degrees of modification by subsequent landslides, erosional processes, vegetation growth and anthropic influences [59]. Therefore, application of multi-temporal high-resolution satellite images for interpretation of smaller landslides may be an effective supplement to the current landslide inventory and efficient for improving the accuracies of landslide susceptibility maps.

According to the existing literature and multicollinearity analysis, sixteen conditioning factors were selected: slope angle, slope aspect, elevation, plan curvature, profile curvature, TWI, STI, SPI, distance to rivers, distance to roads, distance to faults, NDVI, soil, land use, lithology, and rainfall. Furthermore, based on the  $W_f$  values, the relationships between landslide occurrence and these factors were analyzed. It was demonstrated that all factors had nonlinear relationships with landslides. In addition, the RF model was employed to measure the importance of factors with two indices, the MDA and MDG. In terms of MDA, it could be observed that the most critical factor was land use, followed by soil and elevation. Slope angle had the lowest impact on landslide occurrence. However, for MDG, the importance of elevation, rainfall, and land use ranked first, second, and third, respectively, while the lowest MDG value was for profile curvature.

There are some classification techniques for a landslide susceptibility map in GIS software, such as manual, defined interval, natural break, equal interval, quantile, standard deviation, geometrical interval, and landslide percentage [118]. Generally, user-defined classification is more difficult for the reader to interpret and justify. Therefore, current automatic classification systems should be used instead of a user-defined classification [118]. Besides, when landslide susceptibility indexes have positive or negative skewness, the best classification methods are quantile or natural break [119]. In the present study, natural break method, which is the most commonly used models [120,121], is the most suitable method for modelling landslide susceptibility according to the histogram of data distribution.

In this paper, a comparison study of the WoE, WoE-LR, and WoE-RF models was implemented. LR is a widely used model for classification, particularly for binary classification problems [122]. Thus, we integrated the WoE with the LR model to acquire a better classifier. The WoE-RF model is a combination of the weight of evidence and random forest approach. It has been proven that RF is one of the most popular classification algorithms and can improve the performance of single classifiers [96,123]. Moreover, RF can decrease the dependence of the WoE model on independence among the conditioning factors. Accordingly, the results showed that both the LR model (AUC = 0.773 for training data; AUC = 0.763 for validation data) and RF model (AUC = 0.802 for training data; AUC = 0.782 for validation data) can increase the performance of the traditional WoE model (AUC = 0.720 for training data; AUC = 0.695 for validation data), and the WoE-RF model produced the best results.

Comparing the overall classification results of the three models, the results confirmed that the RF model had a better performance on improving the generalization ability of a weak classifier and raising the corresponding prediction accuracy. Therefore, the landslide susceptibility maps generated by the WoE-RF and WoE-LR models contain reference meaning for the study area to a certain extent. Furthermore, the procedure of factor selection and ensemble model construction is of some value to similar studies.

## 6. Conclusions

The results are indicative of the quality of the maps drawn by the hybrid approaches of traditional bivariate weights of evidence (WoE) with multivariate logistic regression (WoE-LR) and machine learning-based random forest (WoE-RF). In general, the following conclusions can be drawn:

(1) Geomorphological factors, geological factors, geo-environmental factors, and anthropogenic factors were used for the development of the landslide model. The preliminary selection of these 16 conditioning factors was based on the multicollinearity diagnosis. The TOL and VIF values of all the conditioning factors indicated no multicollinearity.

(2) According to the results of the WoE model, most occurred at slopes of 10–20° with the south aspect, elevations of 600–800 m, distance to rivers of <200 m, distance to roads of <300 m, and a farmland land cover category.

(3) WoE-RF possessed relatively good accuracy when compared to the WoE-LR and WoE models. By using the ROC curve, the AUC values of the training dataset produced by these three methods were 0.802, 0.773, and 0.720, respectively. For the validation dataset, the AUC values were 0.782, 0.763, and 0.695, respectively. It can be concluded that the proposed hybrid models are promising approaches for the spatial prediction of landslides and can also be applied in other landslide-prone areas.

**Author Contributions:** W.C. and Z.S. collected the field data and conducted the landslide mapping and analysis. W.C. and Z.S. wrote the manuscript. J.H. provided critical comments in planning this paper and edited the manuscript. All authors discussed the results and edited the manuscript.

**Acknowledgments:** This study was supported by the Opening Fund of Key Laboratory of Degraded and Unused Land Consolidation Engineering, the Ministry of Land and Resources (Grant No. SXDJ2018-04), the National Natural Science Foundation of China (Grant No. 41807192), the China Postdoctoral Science Foundation (Grant No. 2018T111084, 2017M613168), and the Project funded by the Shaanxi Province Postdoctoral Science Foundation (Grant No. 2017BSHYDZZ07).

**Conflicts of Interest:** No potential conflict of interest was reported by the authors.

## References

1. Kim, M.S.; Onda, Y.; Kim, J.K.; Kim, S.W. Effect of topography and soil parameterisation representing soil thicknesses on shallow landslide modelling. *Quat. Int.* **2015**, *384*, 91–106. [[CrossRef](#)]
2. Liucci, L.; Melelli, L.; Suteanu, C.; Ponziani, F. The role of topography in the scaling distribution of landslide areas: A cellular automata modeling approach. *Geomorphology* **2017**, *290*, 236–249. [[CrossRef](#)]
3. Agostini, A.; Tofani, V.; Nolesini, T.; Gigli, G.; Tanteri, L.; Rosi, A.; Cardellini, S.; Casagli, N. A new appraisal of the ancona landslide based on geotechnical investigations and stability modelling. *Q. J. Eng. Geol. Hydrogeol.* **2014**, *47*, 29–43. [[CrossRef](#)]
4. Peng, D.; Xu, Q.; Liu, F.; He, Y.; Zhang, S.; Qi, X.; Zhao, K.; Zhang, X. Distribution and failure modes of the landslides in heitai terrace, china. *Eng. Geol.* **2018**, *236*, 97–110. [[CrossRef](#)]
5. Persichillo, M.G.; Bordoni, M.; Meisina, C. The role of land use changes in the distribution of shallow landslides. *Sci. Total Environ.* **2017**, *574*, 924–937. [[CrossRef](#)] [[PubMed](#)]
6. Chang, J.-M.; Chen, H.; Jou, B.J.-D.; Tsou, N.-C.; Lin, G.-W. Characteristics of rainfall intensity, duration, and kinetic energy for landslide triggering in taiwan. *Eng. Geol.* **2017**, *231*, 81–87. [[CrossRef](#)]
7. Segoni, S.; Rosi, A.; Lagomarsino, D.; Fanti, R.; Casagli, N. Brief communication: Using averaged soil moisture estimates to improve the performances of a regional-scale landslide early warning system. *Nat. Hazards Earth Syst. Sci.* **2018**, *18*, 807–812. [[CrossRef](#)]
8. Hou, X.; Vanapalli, S.K.; Li, T. Water infiltration characteristics in loess associated with irrigation activities and its influence on the slope stability in heifangtai loess highland, china. *Eng. Geol.* **2018**, *234*, 27–37. [[CrossRef](#)]
9. Wang, T.; Wu, S.R.; Shi, J.S.; Xin, P.; Wu, L.Z. Assessment of the effects of historical strong earthquakes on large-scale landslide groupings in the wei river midstream. *Eng. Geol.* **2018**, *235*, 11–19. [[CrossRef](#)]
10. Mohammadi, S.; Taiebat, H. Finite element simulation of an excavation-triggered landslide using large deformation theory. *Eng. Geol.* **2016**, *205*, 62–72. [[CrossRef](#)]

11. Alvioli, M.; Melillo, M.; Guzzetti, F.; Rossi, M.; Palazzi, E.; von Hardenberg, J.; Brunetti, M.T.; Peruccacci, S. Implications of climate change on landslide hazard in central italy. *Sci. Total Environ.* **2018**, *630*, 1528–1543. [[CrossRef](#)] [[PubMed](#)]
12. Peres, D.J.; Cancelliere, A. Modeling impacts of climate change on return period of landslide triggering. *J. Hydrol.* **2018**, *567*, 420–434. [[CrossRef](#)]
13. Gariano, S.L.; Guzzetti, F. Landslides in a changing climate. *Earth-Sci. Rev.* **2016**, *162*, 227–252. [[CrossRef](#)]
14. Fell, R.; Corominas, J.; Bonnard, C.; Cascini, L.; Leroi, E.; Savage, W.Z. Guidelines for landslide susceptibility, hazard and risk zoning for land use planning. *Eng. Geol.* **2008**, *102*, 85–98. [[CrossRef](#)]
15. Corominas, J.; van Westen, C.; Frattini, P.; Cascini, L.; Malet, J.P.; Fotopoulou, S.; Catani, F.; Van Den Eeckhaut, M.; Mavrouli, O.; Agliardi, F.; et al. Recommendations for the quantitative analysis of landslide risk. *Bull. Eng. Geol. Environ.* **2014**, *73*, 209–263. [[CrossRef](#)]
16. Pourghasemi, H.R.; Teimoori Yansari, Z.; Panagos, P.; Pradhan, B. Analysis and evaluation of landslide susceptibility: A review on articles published during 2005–2016 (periods of 2005–2012 and 2013–2016). *Arab. J. Geosci.* **2018**, *11*, 193. [[CrossRef](#)]
17. Lee, S.; Dan, N.T. Probabilistic landslide susceptibility mapping in the lai chau province of vietnam: Focus on the relationship between tectonic fractures and landslides. *Environ. Geol.* **2005**, *48*, 778–787. [[CrossRef](#)]
18. Chen, W.; Pourghasemi, H.R.; Panahi, M.; Kornejady, A.; Wang, J.; Xie, X.; Cao, S. Spatial prediction of landslide susceptibility using an adaptive neuro-fuzzy inference system combined with frequency ratio, generalized additive model, and support vector machine techniques. *Geomorphology* **2017**, *297*, 69–85. [[CrossRef](#)]
19. Xu, C.; Xu, X.; Lee, Y.H.; Tan, X.; Yu, G.; Dai, F. The 2010 yushu earthquake triggered landslide hazard mapping using gis and weight of evidence modeling. *Environ. Earth Sci.* **2012**, *66*, 1603–1616. [[CrossRef](#)]
20. Xie, Z.; Chen, G.; Meng, X.; Zhang, Y.; Qiao, L.; Tan, L. A comparative study of landslide susceptibility mapping using weight of evidence, logistic regression and support vector machine and evaluated by sbas-insar monitoring: Zhouqu to wudu segment in bailong river basin, china. *Environ. Earth Sci.* **2017**, *76*, 313. [[CrossRef](#)]
21. Mandal, S.; Mandal, K. Bivariate statistical index for landslide susceptibility mapping in the rorachu river basin of eastern sikkim himalaya, india. *Spat. Inf. Res.* **2018**, *26*, 59–75. [[CrossRef](#)]
22. Regmi, A.D.; Devkota, K.C.; Yoshida, K.; Pradhan, B.; Pourghasemi, H.R.; Kumamoto, T.; Akgun, A. Application of frequency ratio, statistical index, and weights-of-evidence models and their comparison in landslide susceptibility mapping in central nepal himalaya. *Arab. J. Geosci.* **2014**, *7*, 725–742. [[CrossRef](#)]
23. Jaafari, A.; Najafi, A.; Pourghasemi, H.R.; Rezaeian, J.; Sattarian, A. Gis-based frequency ratio and index of entropy models for landslide susceptibility assessment in the caspian forest, northern iran. *Int. J. Environ. Sci. Technol.* **2014**, *11*, 909–926. [[CrossRef](#)]
24. Tien Bui, D.; Shahabi, H.; Shirzadi, A.; Chapi, K.; Alizadeh, M.; Chen, W.; Mohammadi, A.; Ahmad, B.; Panahi, M.; Hong, H.; et al. Landslide detection and susceptibility mapping by airsar data using support vector machine and index of entropy models in cameron highlands, malaysia. *Remote Sens.* **2018**, *10*, 1527. [[CrossRef](#)]
25. Hong, H.; Chen, W.; Xu, C.; Youssef, A.M.; Pradhan, B.; Tien Bui, D. Rainfall-induced landslide susceptibility assessment at the chongren area (china) using frequency ratio, certainty factor, and index of entropy. *Geocarto Int.* **2017**, *32*, 139–154. [[CrossRef](#)]
26. Chen, W.; Li, W.; Chai, H.; Hou, E.; Li, X.; Ding, X. Gis-based landslide susceptibility mapping using analytical hierarchy process (ahp) and certainty factor (cf) models for the baozhong region of baoji city, china. *Environ. Earth Sci.* **2016**, *75*, 1–14. [[CrossRef](#)]
27. Dou, J.; Oguchi, T.; Hayakawa, Y.S.; Uchiyama, S.; Saito, H.; Paudel, U. Gis-based landslide susceptibility mapping using a certainty factor model and its validation in the chuetsu area, central japan. In *Landslide Science for a Safer Geoenvironment*; Springer: New York, NY, USA, 2014; pp. 419–424.
28. Chen, W.; Shahabi, H.; Shirzadi, A.; Hong, H.; Akgun, A.; Tian, Y.; Liu, J.; Zhu, A.-X.; Li, S. Novel hybrid artificial intelligence approach of bivariate statistical-methods-based kernel logistic regression classifier for landslide susceptibility modeling. *Bull. Eng. Geol. Environ.* **2018**, 1–23. [[CrossRef](#)]
29. Pradhan, A.M.S.; Kim, Y.-T. Spatial data analysis and application of evidential belief functions to shallow landslide susceptibility mapping at mt. Umyeon, seoul, korea. *Bull. Eng. Geol. Environ.* **2017**, *76*, 1263–1279. [[CrossRef](#)]

30. Ding, Q.; Chen, W.; Hong, H. Application of frequency ratio, weights of evidence and evidential belief function models in landslide susceptibility mapping. *Geocarto Int.* **2017**, *32*, 619–639. [[CrossRef](#)]
31. Zhang, T.; Han, L.; Chen, W.; Shahabi, H. Hybrid integration approach of entropy with logistic regression and support vector machine for landslide susceptibility modeling. *Entropy* **2018**, *20*, 884. [[CrossRef](#)]
32. Mandal, S.; Mandal, K. Modeling and mapping landslide susceptibility zones using gis based multivariate binary logistic regression (lr) model in the rorachu river basin of eastern sikkim himalaya, india. *Modeling Earth Syst. Environ.* **2018**, *4*, 69–88. [[CrossRef](#)]
33. Chen, W.; Zhang, S.; Li, R.; Shahabi, H. Performance evaluation of the gis-based data mining techniques of best-first decision tree, random forest, and naïve bayes tree for landslide susceptibility modeling. *Sci. Total Environ.* **2018**, *644*, 1006–1018. [[CrossRef](#)]
34. Youssef, A.M.; Pourghasemi, H.R.; Pourtaghi, Z.S.; Al-Katheeri, M.M. Landslide susceptibility mapping using random forest, boosted regression tree, classification and regression tree, and general linear models and comparison of their performance at wadi tayyah basin, asir region, saudi arabia. *Landslides* **2016**, *13*, 839–856. [[CrossRef](#)]
35. Zhou, C.; Yin, K.; Cao, Y.; Ahmed, B.; Li, Y.; Catani, F.; Pourghasemi, H.R. Landslide susceptibility modeling applying machine learning methods: A case study from longju in the three gorges reservoir area, china. *Comput. Geosci.* **2018**, *112*, 23–37. [[CrossRef](#)]
36. Pham, B.T.; Jaafari, A.; Prakash, I.; Bui, D.T. A novel hybrid intelligent model of support vector machines and the multiboost ensemble for landslide susceptibility modeling. *Bull. Eng. Geol. Environ.* **2018**, 1–22. [[CrossRef](#)]
37. Hong, H.; Liu, J.; Bui, D.T.; Pradhan, B.; Acharya, T.D.; Pham, B.T.; Zhu, A.X.; Chen, W.; Ahmad, B.B. Landslide susceptibility mapping using j48 decision tree with adaboost, bagging and rotation forest ensembles in the guangchang area (china). *Catena* **2018**, *163*, 399–413. [[CrossRef](#)]
38. Chen, W.; Shahabi, H.; Shirzadi, A.; Li, T.; Guo, C.; Hong, H.; Li, W.; Pan, D.; Hui, J.; Ma, M.; et al. A novel ensemble approach of bivariate statistical-based logistic model tree classifier for landslide susceptibility assessment. *Geocarto Int.* **2018**, *33*, 1398–1420. [[CrossRef](#)]
39. Chen, W.; Shahabi, H.; Zhang, S.; Khosravi, K.; Shirzadi, A.; Chapi, K.; Pham, B.T.; Zhang, T.; Zhang, L.; Chai, H.; et al. Landslide susceptibility modeling based on gis and novel bagging-based kernel logistic regression. *Appl. Sci.* **2018**, *8*, 2540. [[CrossRef](#)]
40. Truong, X.; Mitamura, M.; Kono, Y.; Raghavan, V.; Yonezawa, G.; Truong, X.; Do, T.; Tien Bui, D.; Lee, S. Enhancing prediction performance of landslide susceptibility model using hybrid machine learning approach of bagging ensemble and logistic model tree. *Appl. Sci.* **2018**, *8*. [[CrossRef](#)]
41. Pham, B.T.; Tien Bui, D.; Prakash, I.; Dholakia, M.B. Hybrid integration of multilayer perceptron neural networks and machine learning ensembles for landslide susceptibility assessment at himalayan area (india) using gis. *CATENA* **2017**, *149*, 52–63. [[CrossRef](#)]
42. Pham, B.T.; Shirzadi, A.; Tien Bui, D.; Prakash, I.; Dholakia, M.B. A hybrid machine learning ensemble approach based on a radial basis function neural network and rotation forest for landslide susceptibility modeling: A case study in the himalayan area, india. *Int. J. Sediment. Res.* **2017**. [[CrossRef](#)]
43. Chen, W.; Pourghasemi, H.R.; Kornejady, A.; Zhang, N. Landslide spatial modeling: Introducing new ensembles of ann, maxent, and svm machine learning techniques. *Geoderma* **2017**, *305*, 314–327. [[CrossRef](#)]
44. Pham, B.T.; Prakash, I.; Tien Bui, D. Spatial prediction of landslides using a hybrid machine learning approach based on random subspace and classification and regression trees. *Geomorphology* **2018**, *303*, 256–270. [[CrossRef](#)]
45. Zabihi, M.; Pourghasemi, H.R.; Pourtaghi, Z.S.; Behzadfar, M. Gis-based multivariate adaptive regression spline and random forest models for groundwater potential mapping in iran. *Environ. Earth Sci.* **2016**, *75*, 665. [[CrossRef](#)]
46. Lagomarsino, D.; Tofani, V.; Segoni, S.; Catani, F.; Casagli, N. A tool for classification and regression using random forest methodology: Applications to landslide susceptibility mapping and soil thickness modeling. *Environ. Modeling Assess.* **2017**, *22*, 201–214. [[CrossRef](#)]
47. Breiman, L. Bagging predictors. *Mach. Learn.* **1996**, *24*, 123–140. [[CrossRef](#)]
48. Tien Bui, D.; Ho, T.-C.; Pradhan, B.; Pham, B.-T.; Nhu, V.-H.; Revhaug, I. Gis-based modeling of rainfall-induced landslides using data mining-based functional trees classifier with adaboost, bagging, and multiboost ensemble frameworks. *Environ. Earth Sci.* **2016**, *75*, 1101. [[CrossRef](#)]

49. Xia, C.-k.; Su, C.-l.; Cao, J.-t.; Li, P. Multiboost with enn-based ensemble fault diagnosis method and its application in complicated chemical process. *J. Cent. South. Univ.* **2016**, *23*, 1183–1197. [[CrossRef](#)]
50. Pham, B.T.; Shirzadi, A.; Tien Bui, D.; Prakash, I.; Dholakia, M.B. A hybrid machine learning ensemble approach based on a radial basis function neural network and rotation forest for landslide susceptibility modeling: A case study in the himalayan area, india. *Int. J. Sediment. Res.* **2018**, *33*, 157–170. [[CrossRef](#)]
51. Fanos, A.M.; Pradhan, B.; Mansor, S.; Yusoff, Z.M.; Abdullah, A.F.B. A hybrid model using machine learning methods and gis for potential rockfall source identification from airborne laser scanning data. *Landslides* **2018**, *15*, 1833–1850. [[CrossRef](#)]
52. Chen, W.; Panahi, M.; Tsangaratos, P.; Shahabi, H.; Ilia, I.; Panahi, S.; Li, S.; Jaafari, A.; Ahmad, B.B. Applying population-based evolutionary algorithms and a neuro-fuzzy system for modeling landslide susceptibility. *CATENA* **2019**, *172*, 212–231. [[CrossRef](#)]
53. Naghibi, S.A.; Moghaddam, D.D.; Kalantar, B.; Pradhan, B.; Kisi, O. A comparative assessment of gis-based data mining models and a novel ensemble model in groundwater well potential mapping. *J. Hydrol.* **2017**, *548*, 471–483. [[CrossRef](#)]
54. Chen, W.; Li, H.; Hou, E.; Wang, S.; Wang, G.; Panahi, M.; Li, T.; Peng, T.; Guo, C.; Niu, C.; et al. Gis-based groundwater potential analysis using novel ensemble weights-of-evidence with logistic regression and functional tree models. *Sci. Total Environ.* **2018**, *634*, 853–867. [[CrossRef](#)] [[PubMed](#)]
55. Kadavi, P.; Lee, C.-W.; Lee, S. Application of ensemble-based machine learning models to landslide susceptibility mapping. *Remote Sens.* **2018**, *10*, 1252. [[CrossRef](#)]
56. Chen, W.; Xie, X.; Peng, J.; Shahabi, H.; Hong, H.; Bui, D.T.; Duan, Z.; Li, S.; Zhu, A.X. Gis-based landslide susceptibility evaluation using a novel hybrid integration approach of bivariate statistical based random forest method. *CATENA* **2018**, *164*, 135–149. [[CrossRef](#)]
57. Vakhshoori, V.; Pourghasemi, H.R. A novel hybrid bivariate statistical method entitled froc for landslide susceptibility assessment. *Environ. Earth Sci.* **2018**, *77*, 686. [[CrossRef](#)]
58. Fell, R.; Glastonbury, J.; Hunter, G. Rapid landslides: The importance of understanding mechanisms and rupture surface mechanics. *Q. J. Eng. Geol. Hydrogeol.* **2007**, *40*, 9–27. [[CrossRef](#)]
59. Rosi, A.; Tofani, V.; Tanteri, L.; Stefanelli, C.T.; Agostini, A.; Catani, F.; Casagli, N. The new landslide inventory of tuscany (italy) updated with ps-insar: Geomorphological features and landslide distribution. *Landslides* **2018**, *15*, 5–19. [[CrossRef](#)]
60. Hungr, O.; Leroueil, S.; Picarelli, L. The varnes classification of landslide types, an update. *Landslides* **2014**, *11*, 167–194. [[CrossRef](#)]
61. Tien Bui, D.; Tuan, T.A.; Klempe, H.; Pradhan, B.; Revhaug, I. Spatial prediction models for shallow landslide hazards: A comparative assessment of the efficacy of support vector machines, artificial neural networks, kernel logistic regression, and logistic model tree. *Landslides* **2016**, *13*, 361–378. [[CrossRef](#)]
62. Dai, F.C.; Lee, C.F.; Li, J.; Xu, Z.W. Assessment of landslide susceptibility on the natural terrain of lantau island, hong kong. *Environ. Geol.* **2001**, *40*, 381–391.
63. Nefeslioglu, H.A.; Duman, T.Y.; Durmaz, S. Landslide susceptibility mapping for a part of tectonic kelkit valley (eastern black sea region of turkey). *Geomorphology* **2008**, *94*, 401–418. [[CrossRef](#)]
64. Pham, B.T.; Khosravi, K.; Prakash, I. Application and comparison of decision tree-based machine learning methods in landside susceptibility assessment at pauri garhwal area, uttarakhand, india. *Environ. Process.* **2017**, *4*, 711–730. [[CrossRef](#)]
65. Wu, Y.; Li, W.; Liu, P.; Bai, H.; Wang, Q.; He, J.; Liu, Y.; Sun, S. Application of analytic hierarchy process model for landslide susceptibility mapping in the gangu county, gansu province, china. *Environ. Earth Sci.* **2016**, *75*, 422. [[CrossRef](#)]
66. Saadatkhah, N.; Kassim, A.; Lee, L.M. Susceptibility assessment of shallow landslides in hulu kelang area, kuala lumpur, malaysia using analytical hierarchy process and frequency ratio. *Geotech. Geol. Eng.* **2015**, *33*, 43–57. [[CrossRef](#)]
67. Aditian, A.; Kubota, T.; Shinohara, Y. Comparison of gis-based landslide susceptibility models using frequency ratio, logistic regression, and artificial neural network in a tertiary region of ambon, indonesia. *Geomorphology* **2018**, *318*, 101–111. [[CrossRef](#)]
68. Riaz Muhammad, T.; Basharat, M.; Hameed, N.; Shafique, M.; Luo, J. A data-driven approach to landslide-susceptibility mapping in mountainous terrain: Case study from the northwest himalayas, pakistan. *Nat. Hazards Rev.* **2018**, *19*, 05018007. [[CrossRef](#)]

69. Chen, W.; Li, W.; Hou, E.; Bai, H.; Chai, H.; Wang, D.; Cui, X.; Wang, Q. Application of frequency ratio, statistical index, and index of entropy models and their comparison in landslide susceptibility mapping for the baozhong region of baoji, china. *Arab. J. Geosci.* **2015**, *8*, 1829–1841. [[CrossRef](#)]
70. Moore, I.D.; Grayson, R.B.; Ladson, A.R. Digital terrain modelling: A review of hydrological, geomorphological, and biological applications. *Hydrol. Process.* **1991**, *5*, 3–30. [[CrossRef](#)]
71. Chen, W.; Peng, J.; Hong, H.; Shahabi, H.; Pradhan, B.; Liu, J.; Zhu, A.-X.; Pei, X.; Duan, Z. Landslide susceptibility modelling using gis-based machine learning techniques for chongren county, jiangxi province, china. *Sci. Total Environ.* **2018**, *626*, 1121–1135. [[CrossRef](#)]
72. Beven, K.J.; Kirkby, M.J. A physically based, variable contributing area model of basin hydrology/un modèle à base physique de zone d'appel variable de l'hydrologie du bassin versant. *Int. Assoc. Sci. Hydrol. Bull.* **1979**, *24*, 43–69. [[CrossRef](#)]
73. Ge, Y.; Chen, H.; Zhao, B.; Tang, H.; Lin, Z.; Xie, Z.; Lv, L.; Zhong, P. A comparison of five methods in landslide susceptibility assessment: A case study from the 330-kv transmission line in gansu region, china. *Environ. Earth Sci.* **2018**, *77*, 662. [[CrossRef](#)]
74. Wu, Z.; Wu, Y.; Yang, Y.; Chen, F.; Zhang, N.; Ke, Y.; Li, W. A comparative study on the landslide susceptibility mapping using logistic regression and statistical index models. *Arab. J. Geosci.* **2017**, *10*, 187. [[CrossRef](#)]
75. Yalcin, A. Gis-based landslide susceptibility mapping using analytical hierarchy process and bivariate statistics in ardesen (turkey): Comparisons of results and confirmations. *CATENA* **2008**, *72*, 1–12. [[CrossRef](#)]
76. Akgun, A. A comparison of landslide susceptibility maps produced by logistic regression, multi-criteria decision, and likelihood ratio methods: A case study at İzmir, turkey. *Landslides* **2012**, *9*, 93–106. [[CrossRef](#)]
77. Chen, W.; Yan, X.; Zhao, Z.; Hong, H.; Bui, D.T.; Pradhan, B. Spatial prediction of landslide susceptibility using data mining-based kernel logistic regression, naive bayes and rbfnetwork models for the long county area (china). *Bull. Eng. Geol. Environ.* **2018**, 1–20. [[CrossRef](#)]
78. Xu, C.; Dai, F.; Xu, X.; Lee, Y.H. Gis-based support vector machine modeling of earthquake-triggered landslide susceptibility in the jianjiang river watershed, China. *Geomorphology* **2012**, *145–146*, 70–80. [[CrossRef](#)]
79. Ohlmacher, G.C.; Davis, J.C. Using multiple logistic regression and gis technology to predict landslide hazard in northeast kansas, USA. *Eng. Geol.* **2003**, *69*, 331–343. [[CrossRef](#)]
80. Al-Abadi, A.M.; Shahid, S. A comparison between index of entropy and catastrophe theory methods for mapping groundwater potential in an arid region. *Environ. Monit. Assess.* **2015**, *187*, 576. [[CrossRef](#)]
81. Salvatici, T.; Tofani, V.; Rossi, G.; D'Ambrosio, M.; Tacconi Stefanelli, C.; Masi, E.B.; Rosi, A.; Pazzi, V.; Vannocci, P.; Petrolo, M.; et al. Application of a physically based model to forecast shallow landslides at a regional scale. *Nat. Hazards Earth Syst. Sci.* **2018**, *18*, 1919–1935. [[CrossRef](#)]
82. Peng, J.; Tong, X.; Wang, S.; Ma, P. Three-dimensional geological structures and sliding factors and modes of loess landslides. *Environ. Earth Sci.* **2018**, *77*, 675. [[CrossRef](#)]
83. Santo, A.; Di Crescenzo, G.; Forte, G.; Papa, R.; Pirone, M.; Urciuoli, G. Flow-type landslides in pyroclastic soils on flysch bedrock in southern italy: The bosco de' preti case study. *Landslides* **2018**, *15*, 63–82. [[CrossRef](#)]
84. Glade, T. Landslide occurrence as a response to land use change: A review of evidence from new zealand. *CATENA* **2003**, *51*, 297–314. [[CrossRef](#)]
85. Cui, S.-H.; Pei, X.-J.; Wu, H.-Y.; Huang, R.-Q. Centrifuge model test of an irrigation-induced loess landslide in the heifangtai loess platform, northwest china. *J. Mt. Sci.* **2018**, *15*, 130–143. [[CrossRef](#)]
86. Justice, C.O.; Townshend, J.R.G.; Holben, B.N.; Tucker, C.J. Analysis of the phenology of global vegetation using meteorological satellite data. *Int. J. Remote Sens.* **1985**, *6*, 1271–1318. [[CrossRef](#)]
87. Chen, W.; Xie, X.; Wang, J.; Pradhan, B.; Hong, H.; Tien Bui, D.; Duan, Z.; Ma, J. A comparative study of logistic model tree, random forest, and classification and regression tree models for spatial prediction of landslide susceptibility. *CATENA* **2017**, *151*, 147–160. [[CrossRef](#)]
88. Peruccacci, S.; Brunetti, M.T.; Luciani, S.; Vennari, C.; Guzzetti, F. Lithological and seasonal control on rainfall thresholds for the possible initiation of landslides in central italy. *Geomorphology* **2012**, *139–140*, 79–90. [[CrossRef](#)]
89. Tsukamoto, Y.; Ohta, T. Runoff process on a steep forested slope. *J. Hydrol.* **1988**, *102*, 165–178. [[CrossRef](#)]
90. Agterberg, F.P. Systematic approach to dealing with uncertainty of geoscience information in mineral exploration. *APCO* **1989**, *89*, 165–178.

91. Dahal, R.K.; Hasegawa, S.; Nonomura, A.; Yamanaka, M.; Masuda, T.; Nishino, K. Gis-based weights-of-evidence modelling of rainfall-induced landslides in small catchments for landslide susceptibility mapping. *Environ. Geol.* **2008**, *54*, 311–324. [[CrossRef](#)]
92. Lachenbruch, P.A.; McCullagh, P.; Nelder, J.A. Generalized linear models. *Biometrics* **1990**, *46*, 291–303. [[CrossRef](#)]
93. Agarwal, S.; Kachroo, P.; Regentova, E. A hybrid model using logistic regression and wavelet transformation to detect traffic incidents. *IATSS Res.* **2016**, *40*, 56–63. [[CrossRef](#)]
94. Ravi, D.; Bober, M.; Farinella, G.M.; Guarnera, M.; Battiato, S. Semantic segmentation of images exploiting dct based features and random forest. *Pattern Recognit.* **2016**, *52*, 260–273. [[CrossRef](#)]
95. Masetic, Z.; Subasi, A. Congestive heart failure detection using random forest classifier. *Comput. Methods Programs Biomed.* **2016**, *130*, 54–64. [[CrossRef](#)] [[PubMed](#)]
96. Breiman, L. Random forests. *Mach. Learn.* **2001**, *45*, 5–32. [[CrossRef](#)]
97. Ozdemir, A. Landslide susceptibility mapping using bayesian approach in the sultan mountains (akşehir, turkey). *Nat. Hazards* **2011**, *59*, 1573–1607. [[CrossRef](#)]
98. Chen, W.; Xie, X.; Peng, J.; Wang, J.; Duan, Z.; Hong, H. Gis-based landslide susceptibility modelling: A comparative assessment of kernel logistic regression, naïve-bayes tree, and alternating decision tree models. *Geomat. Nat. Hazards Risk* **2017**, *8*, 950–973. [[CrossRef](#)]
99. Lin, G.-F.; Chang, M.-J.; Huang, Y.-C.; Ho, J.-Y. Assessment of susceptibility to rainfall-induced landslides using improved self-organizing linear output map, support vector machine, and logistic regression. *Eng. Geol.* **2017**, *224*, 62–74. [[CrossRef](#)]
100. Lee, J.-H.; Sameen, M.I.; Pradhan, B.; Park, H.-J. Modeling landslide susceptibility in data-scarce environments using optimized data mining and statistical methods. *Geomorphology* **2018**, *303*, 284–298. [[CrossRef](#)]
101. Yu, H.; Jiang, S.; Land, K.C. Multicollinearity in hierarchical linear models. *Soc. Sci. Res.* **2015**, *53*, 118–136. [[CrossRef](#)]
102. Ozdemir, A.; Altural, T. A comparative study of frequency ratio, weights of evidence and logistic regression methods for landslide susceptibility mapping: Sultan mountains, sw turkey. *J. Asian Earth Sci.* **2013**, *64*, 180–197. [[CrossRef](#)]
103. Ozdemir, A. Gis-based groundwater spring potential mapping in the sultan mountains (konya, turkey) using frequency ratio, weights of evidence and logistic regression methods and their comparison. *J. Hydrol.* **2011**, *411*, 290–308. [[CrossRef](#)]
104. Hong, H.; Tsangaratos, P.; Ilia, I.; Chen, W.; Xu, C. Comparing the Performance of a Logistic Regression and a Random Forest Model in Landslide Susceptibility Assessments. the Case of Wuyuan Area, China. In *Workshop on World Landslide Forum*; Mikos, M., Tiwari, B., Yin, Y., Eds.; Springer: Cham, Switzerland, 2017; pp. 1043–1050.
105. Pham, B.T.; Pradhan, B.; Tien Bui, D.; Prakash, I.; Dholakia, M.B. A comparative study of different machine learning methods for landslide susceptibility assessment: A case study of uttarakhand area (india). *Environ. Model. Softw.* **2016**, *84*, 240–250. [[CrossRef](#)]
106. Tien Bui, D.; Tuan, T.A.; Hoang, N.-D.; Thanh, N.Q.; Nguyen, D.B.; Van Liem, N.; Pradhan, B. Spatial prediction of rainfall-induced landslides for the lao cai area (vietnam) using a hybrid intelligent approach of least squares support vector machines inference model and artificial bee colony optimization. *Landslides* **2017**, *14*, 447–458. [[CrossRef](#)]
107. Chen, W.; Pourghasemi, H.R.; Naghibi, S.A. Prioritization of landslide conditioning factors and its spatial modeling in shangnan county, china using gis-based data mining algorithms. *Bull. Eng. Geol. Environ.* **2018**, *77*, 611–629. [[CrossRef](#)]
108. Chen, W.; Pourghasemi, H.R.; Naghibi, S.A. A comparative study of landslide susceptibility maps produced using support vector machine with different kernel functions and entropy data mining models in china. *Bull. Eng. Geol. Environ.* **2018**, *77*, 647–664. [[CrossRef](#)]
109. He, S.; Pan, P.; Dai, L.; Wang, H.; Liu, J. Application of kernel-based fisher discriminant analysis to map landslide susceptibility in the qinggan river delta, three gorges, china. *Geomorphology* **2012**, *171*, 30–41. [[CrossRef](#)]
110. Chen, W.; Panahi, M.; Pourghasemi, H.R. Performance evaluation of gis-based new ensemble data mining techniques of adaptive neuro-fuzzy inference system (anfis) with genetic algorithm (ga), differential evolution

- (de), and particle swarm optimization (pso) for landslide spatial modelling. *CATENA* **2017**, *157*, 310–324. [[CrossRef](#)]
111. Wang, Q.; Li, W.; Wu, Y.; Pei, Y.; Xie, P. Application of statistical index and index of entropy methods to landslide susceptibility assessment in gongliu (xinjiang, china). *Environ. Earth Sci.* **2016**, *75*, 599. [[CrossRef](#)]
  112. Naghibi, S.A.; Ahmadi, K.; Daneshi, A. Application of support vector machine, random forest, and genetic algorithm optimized random forest models in groundwater potential mapping. *Water Resour. Manag.* **2017**, *31*, 2761–2775. [[CrossRef](#)]
  113. Chen, W.; Shirzadi, A.; Shahabi, H.; Ahmad, B.B.; Zhang, S.; Hong, H.; Zhang, N. A novel hybrid artificial intelligence approach based on the rotation forest ensemble and naïve bayes tree classifiers for a landslide susceptibility assessment in langao county, china. *Geomat. Nat. Hazards Risk* **2017**, *8*, 1955–1977. [[CrossRef](#)]
  114. Ilia, I.; Tsangaratos, P. Applying weight of evidence method and sensitivity analysis to produce a landslide susceptibility map. *Landslides* **2016**, *13*, 379–397. [[CrossRef](#)]
  115. Polykretis, C.; Chalkias, C. Comparison and evaluation of landslide susceptibility maps obtained from weight of evidence, logistic regression, and artificial neural network models. *Nat. Hazards* **2018**. [[CrossRef](#)]
  116. Lee, S. Landslide detection and susceptibility mapping in the sagimakri area, korea using kompsat-1 and weight of evidence technique. *Environ. Earth Sci.* **2013**, *70*, 3197–3215. [[CrossRef](#)]
  117. Malamud, B.D.; Turcotte, D.L.; Guzzetti, F.; Reichenbach, P. Landslide inventories and their statistical properties. *Earth Surf. Process. Landf.* **2004**, *29*, 687–711. [[CrossRef](#)]
  118. Baeza, C.; Lantada, N.; Amorim, S. Statistical and spatial analysis of landslide susceptibility maps with different classification systems. *Environ. Earth Sci.* **2016**, *75*, 1318. [[CrossRef](#)]
  119. Akgun, A.; Sezer, E.A.; Nefeslioglu, H.A.; Gokceoglu, C.; Pradhan, B. An easy-to-use matlab program (mamland) for the assessment of landslide susceptibility using a mamdani fuzzy algorithm. *Comput. Geosci.* **2012**, *38*, 23–34. [[CrossRef](#)]
  120. Kumar, R.; Anbalagan, R. Landslide susceptibility mapping using analytical hierarchy process (ahp) in tehri reservoir rim region, uttarakhand. *J. Geol. Soc. India* **2016**, *87*, 271–286. [[CrossRef](#)]
  121. Khosravi, K.; Pourghasemi, H.R.; Chapi, K.; Bahri, M. Flash flood susceptibility analysis and its mapping using different bivariate models in iran: A comparison between shannon('s entropy, statistical index, and weighting factor models. *Environ. Monit. Assess.* **2016**, *188*, 656. [[CrossRef](#)] [[PubMed](#)]
  122. Kleinbaum, D.G.; Klein, M. Introduction to logistic regression. In *Logistic Regression: A Self-Learning Text*; Kleinbaum, D.G., Ed.; Springer: New York, NY, USA, 2010.
  123. Genuer, R.; Poggi, J.-M.; Tuleau-Malot, C.; Villa-Vialaneix, N. Random forests for big data. *Big Data Res.* **2017**, *9*, 28–46. [[CrossRef](#)]



© 2019 by the authors. Licensee MDPI, Basel, Switzerland. This article is an open access article distributed under the terms and conditions of the Creative Commons Attribution (CC BY) license (<http://creativecommons.org/licenses/by/4.0/>).